# Measurement report: Atmospheric nitrate radical chemistry in the South China Sea influenced by the urban outflow of the Pearl River Delta

Jie Wang[1, 2], Haichao Wang[1, 2 *], Yee Jun Tham[3, 4 *], Lili Ming[5], Zelong Zheng[1], Guizhen Fang[3], Cuizhi Sun[1, 2], Zhenhao Ling[1, 2], Jun Zhao[1, 2], Shaojia Fan[1, 2]

[1] School of Atmospheric Sciences, Sun Yat-sen University, and Southern Marine Science and Engineering Guangdong Laboratory (Zhuhai), Zhuhai, 519082, China
[2] Guangdong Provincial Observation and Research Station for Climate Environment and Air Quality Change in the Pearl River Estuary, Key Laboratory of Tropical Atmosphere-Ocean System (Sun Yat-sen University), Ministry of Education, Zhuhai, 519082, China
[3] School of Marine Sciences, Sun Yat-sen University, Zhuhai 519082, China.
[4] Pearl River Estuary Marine Ecosystem Research Station, Ministry of Education, Zhuhai, 519082, China.
[5] Technical Center of Gongbei Customs District of China, Zhuhai, 519000, China.

*Correspondence to:* Haichao Wang (wanghch27@mail.sysu.edu.cn); Yee Jun Tham (thamyj@mail.sysu.edu.cn)

**Abstract.** Nitrate radical ($NO_3$) is a critical nocturnal atmospheric oxidant in the troposphere, which widely affects the fate of air pollutants and regulates air quality. Many previous works have reported the chemistry of $NO_3$ in inland regions of China, while fewer studies target marine regions. Here, we present a field measurement of the $NO_3$ reservoir, dinitrogen pentoxide ($N_2O_5$), and related species at a typical marine site (Da Wan Shan Island) located in the South China Sea in the winter of 2021. Two patterns of air masses were captured during the campaign, including the dominant airmass from inland China (IAM) with a percentage of ~84%, and the airmass from eastern coastal areas (CAM) with ~16%. During the IAM period, the $NO_3$ production rate reached 1.6 ± 0.9 ppbv $h^{-1}$ due to the transportation of the polluted urban plume with high $NO_x$ and $O_3$. While the average nocturnal $N_2O_5$ and the calculated $NO_3$ mixing ratio were 119.5 ± 128.6 pptv and 9.9 ± 12.5 pptv, respectively, and the steady state lifetime of $NO_3$ was 0.5 ± 0.7 min on average, indicating intensive nighttime chemistry and rapid $NO_3$ loss at this site. By examining the reaction of $NO_3$ with volatile organic compounds (VOCs) and $N_2O_5$ heterogeneous hydrolysis, we revealed that these two reaction pathways were not responsible for the $NO_3$ loss (<20%), since the $NO_3$ reactivity ($k(NO_3)$) towards VOCs was small ($5.2\times10^{-3}$ $s^{-1}$)

and the aerosol loading was low. Instead, NO was proposed to significantly contribute to nocturnal $NO_3$ loss at this site, despite the nocturnal NO concentration always at sub-ppbv level and near the instrument detection limit. It might be from the local soil emission or others. We infer that the nocturnal chemical $NO_3$ reactions would be largely enhanced once without NO emission in the open ocean after the air mass passes through this site, thus highlighting the strong influences of the urban outflow to the downwind marine areas in terms of nighttime chemistry. During the CAM period, nocturnal ozone was higher, while $NO_x$ was much lower. The $NO_3$ production was still very fast, with a rate of 1.2 ppbv $h^{-1}$. With the absence of $N_2O_5$ measurement in this period, the $NO_3$ reactivity towards VOCs and $N_2O_5$ uptake were calculated to assess $NO_3$ loss processes. We showed that the average k($NO_3$) from VOCs (56.5%, $2.6 \pm 0.9 \times 10^{-3}$ $s^{-1}$) was higher than that from $N_2O_5$ uptake (43.5%, $2.0 \pm 1.5 \times 10^{-3}$ $s^{-1}$) during the CAM period, indicating a longer $NO_3$/$N_2O_5$ lifetime than that during IAM period. This study improves the understanding of the nocturnal $NO_3$ budget and environmental impacts with the interaction of anthropogenic and natural activities in marine regions.

## 1. Introduction

Reactive nitrogen compounds, especially the nitrate radical ($NO_3$) and dinitrogen pentoxide ($N_2O_5$) play an essential role in nocturnal atmospheric chemistry (Wayne et al., 1991; Brown and Stutz, 2012). $NO_3$ is mainly generated via the oxidation of $NO_2$ by $O_3$ (R1), and then $NO_3$ further reacts with $NO_2$ to produce $N_2O_5$ (R2) with a thermal equilibrium. The temperature-dependent equilibrium constant, $K_{eq}$, regulates the equilibrium favoring $NO_3$ and $NO_2$ at higher temperatures (Osthoff et al., 2007; Chen et al., 2022). During daytime, the $NO_3$ mixing ratio is generally low as its lifetime is very short (< 5 s) due to the fast photolysis (R3) and rapid reaction with NO (R4) (a rate constant of $2.6 \times 10^{-11}$ $cm^3$ $molecule^{-1}$ $s^{-1}$ at 298 K, Atkinson et al., 2004). While at night, $NO_3$ accumulates and can reach tens to hundreds of parts per trillion by volume (pptv), making it the major nocturnal oxidizing agent (Wang et al., 2015).

$$NO_2 + O_3 \rightarrow NO_3 + O_2 \quad \text{(R1)}$$

$$NO_2 + NO_3 \rightleftharpoons N_2O_5 \quad \text{(R2)}$$

$$NO_3 + h\nu \rightarrow NO_2 + NO \quad \text{(R3)}$$

$$NO + NO_3 \rightarrow 2NO_2 \quad \text{(R4)}$$

During nighttime, $NO_3$ is the most important oxidant for alkenes (Mogensen et al., 2015; Edwards et al., 2017), particularly in rural, remote, or forested environments, where it predominantly reacts with unsaturated biogenic volatile organic compounds (VOCs), especially isoprene and monoterpene (Ng et al., 2017; Liebmann et al., 2018b; Liebmann et al., 2018a), to form alkyl nitrates ($RONO_2$), that ultimately lead to secondary organic aerosols (SOAs) (Brown and Stutz, 2012). The observations and model simulations showed that the measured particulate organic nitrates were largely attributed to the nocturnal $NO_3$ oxidation across Europe (Kiendler-Scharr et al., 2016). The $NO_3$ oxidation was also reported to play an important role in aerosol formation in the Southeastern United States with high isoprene and monoterpene emissions (Xu et al., 2015). These studies highlighted the critical role of the reaction of $NO_3$ with VOCs in $NO_3$ budget and organic aerosol pollution. In addition, $NO_3$ also reacts with dimethyl sulfide (DMS) over the ocean, affecting the marine sulfur cycle and thus cloud formation and global climate (Aldener et al., 2006; Brown and Stutz, 2012; Ian Barnes et al., 2006; Rosati et al., 2022). While in high aerosol loading regimes, the $N_2O_5$ heterogeneous uptake becomes a significant indirect $NO_3$ loss pathway. The hydrolysis reaction produces nitrate ($NO_3^-$) and nitryl chloride ($ClNO_2$) on chloride-containing aerosol surfaces (Osthoff et al., 2008; Thornton et al., 2010), in which $ClNO_2$ activates the Cl radical and further enhances the photochemistry and ozone pollution in the following day (Riedel et al., 2012; Riedel et al., 2014; Behnke et al., 1993).

Different $NO_3$ loss pathways produce different air pollutants, thus characterization of $NO_3$ budget is essential to clarify the $NO_3$ chemistry in air pollution under various environments. Observations of $N_2O_5$ and $NO_3$ in different regions and evaluation of their loss processes have been reported in numerous studies (Crowley et al., 2011; Geyer et al., 2001; Brown et al., 2011; Dewald et al., 2022; Niu et al., 2022; Brown et al., 2016; Wang et al., 2020a; Tham et al., 2016; Aldener et al., 2006; Lin et al., 2022). In general, the $NO_3$ loss process shows significant regional differences. In urban areas featuring intensive anthropogenic $NO_x$ emissions and moderate (or high) aerosol loading, $N_2O_5$ uptake is comparable or even dominates the $NO_3$ loss (Wang et al., 2013). While in rural and forested areas with abundant biogenic VOC (BVOC) emissions, the $NO_3$ loss processes were usually dominated by BVOCs (Dewald et al., 2022; Geyer et al., 2001; Brown et al., 2011). As for the coastal areas, which were jointly affected by the polluted air mass from the inland and the relatively clean air mass from the ocean, the dominant $NO_3$ loss process varies greatly depending on the air mass origin (Aldener et al., 2006; Niu et al., 2022; Brown et al., 2016; Crowley et al., 2011). For instance, Crowley et al. (2011) found in the Atlantic coast of Southern Spain (forested area) that when the air mass mainly originated from the Atlantic, $NO_3$ was mainly consumed by BVOCs (mainly monoterpenes) emitted from nearby forests, while when the air mass came from the continent, $NO_3$ loss was mainly due to reactions with anthropogenic

VOCs (AVOCs).

China has been recently proven to be a hot spot of nocturnal chemistry with a high $NO_3$ production rate (Wang et al., 2023). Many studies have reported the mechanisms, budget, or impacts of $NO_3$-$N_2O_5$ chemistry in different regions, while most of them were conducted in urban regions (Wang et al., 2013; Yan et al., 2021; Wang et al., 2020a; Wang et al., 2017c; Wang et al., 2017d). For example, Wang et al. (2017b) showed a significant contribution of $N_2O_5$ uptake to nitrate pollution in summer and winter, and they also highlighted the fast organic nitrate production rate observed in Beijing rural region in summer (Wang et al., 2018b). Only several studies focused on nighttime oxidation in coastal cities like Shanghai, Shenzhen, and Hong Kong (Zhu et al., 2022; Niu et al., 2022; Yan et al., 2019), which showed different patterns of $NO_3$ chemistry compared with urban regions. Even fewer field studies were conducted on the island which is far away from the coastal cities where the interactions of the oceanic atmosphere and urban plumes can significantly affect the $NO_3$ budget and impacts. Given the diversity of air masses in inland and coastal areas, studies are needed to gain a comprehensive understanding of $NO_3$ losses in different atmospheric environments, particularly in coastal and marine areas.

Therefore, we conducted an intensive field observation on Da Wan Shan Island (DWS) in the winter of 2021, which is a typical island site in the north of the South China Sea, and downwind of the city clusters in the Pearl River Delta, China during the winter monsoon periods. The island features a subtropical oceanic monsoon climate, and the north and northeast synoptic winds from inland PRD and eastern China coast are generally predominant in winter (Liu et al., 2019; Wang et al., 2018a). This allows us to further investigate the interactions between anthropogenic emissions and marine emissions from the perspective of nighttime chemistry. In this study, the measurements of $N_2O_5$ and the related species during the DWS winter campaign are reported. We have identified two types of air masses from both mainland China and coastal areas. Finally, the $NO_3$ budget and loss processes in different air masses are characterized.

## 2. Methods

### 2.1 Site description

The field campaign was conducted at Da Wan Shan Island (21°55′57″ N, 113°43′15″ E) from Nov. 9$^{th}$ to Dec. 16$^{th}$, 2021. Fig. 1 shows the location of the study site, which is approximately 60 km southwest of Hong Kong; 40 km southeast of Zhuhai; and about 100 km and 80 km away from the megacities Guangzhou and Shenzhen, respectively. This island is dominated by mountainous terrain with an area of 8.1 km$^2$ and has a small

population of about 3,000. Anthropogenic emissions are sparse and no industrial pollution sources were identified, though numerous ships engaging in local fishing activities were observed, potentially affecting the local atmosphere. During the measurement, local airflow was consistently from either the northwest or southeast (Fig. 1a) due to the winter monsoon, with wind speeds most frequently ranging from 1.8 to 7.9 m $s^{-1}$ ($10^{th}$ - $90^{th}$ percentiles) and an average of 4.5 ± 2.6 m $s^{-1}$. This wind direction is indicative of the mixing of air masses from both continental and coastal areas. The Hybrid Single-Particle Lagrangian Integrated Trajectory model (HYSPLIT) was adopted to investigate the historical trajectory. The HYSPLIT model was run for 48 hours backward in time at local times of 20:00, 24:00, and 04:00, and at a height of 70 m above sea level. It confirmed that the airmass during nighttime mostly came from inland China (fresh urban emissions, IAM, 84%) and the coastal areas (aged urban emissions, CAM, 16%). IAM featured the outflow from inland China, such as Guangzhou and Changsha, while CAM featured the outflow of coastal cities like Hong Kong and Shenzhen. No air masses free of pollution from the South China Sea were observed during the measurement period. All measurement instruments were placed in the DWS Atmospheric-Marine Research Station, located on the rooftop with inlets approximately 10 m above ground level and about 72 m above sea level. All times were given in CNST (Chinese National Standard Time = UTC + 8 h), with sunrise around 06:40 CNST and sunset at 17:40 CNST.

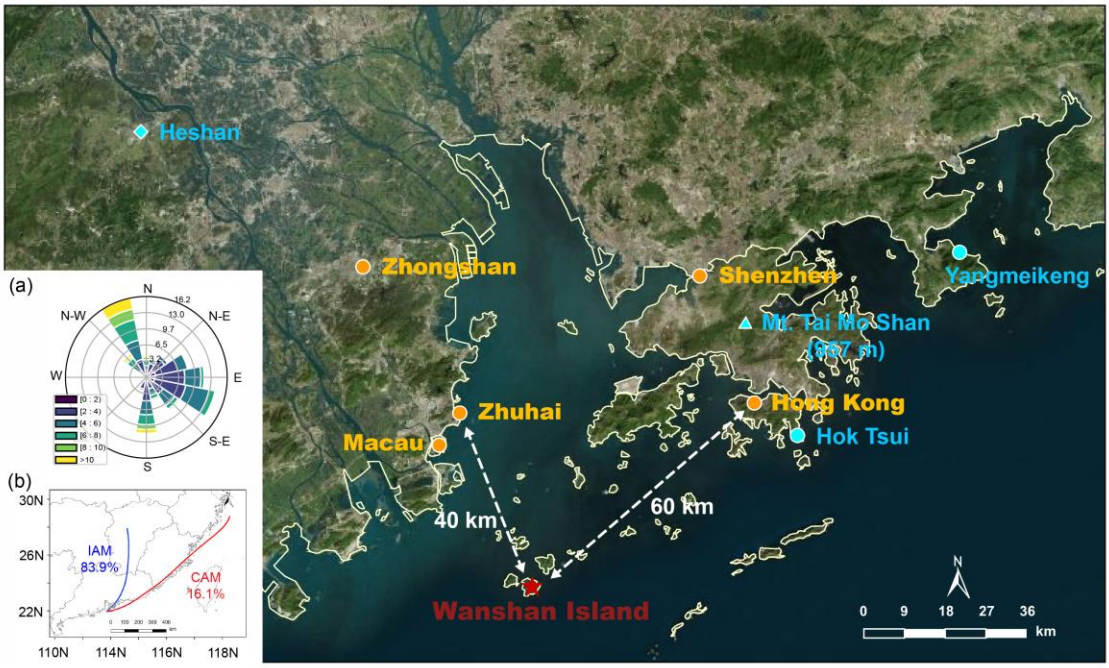


**Figure 1.** A map of the field measurement site of Wanshan Island (red star) and the surrounding environment (extracted from BingSatelliteMap). Two coastal sites Hok Tsui

(Yan et al., 2019) and Yangmeikeng (Niu et al., 2022), and an urban site Heshan (Wang et al., 2022; Yun et al., 2018b) are denoted as blue circle and diamond, respectively. The blue triangle denoted Mt. Tai Mo Shan (957 m), a mountainous site that studied the nighttime chemistry in the nocturnal residual layer (Brown et al., 2016). The inset plot (a) provides the wind rose for the sampling site during the campaign. Panel (b) shows the clustering result of the 48-hrs backward trajectory calculations at nighttime using the HYSPLIT model throughout the campaign.

## 2.2 Instrument setup

Various parameters were measured in this study, including $N_2O_5$, NO, $NO_2$, $O_3$, VOCs, particle number size distribution (PNSD), and meteorological parameters with different instruments. The detail information about these instruments is listed in Table 1. The $N_2O_5$ measurements were performed using a cavity-enhanced absorption spectrometer (CEAS) which has been deployed in several field campaigns (Wang et al., 2017a; Wang et al., 2017b; Wang et al., 2018b; Wang et al., 2020b). In brief, ambient $N_2O_5$ was thermally decomposed to $NO_3$ in a perfluoro alkoxy alkane (PFA) tube (length: 35 cm, I.D.: 4.35 mm) heated to 130 ℃, and $NO_3$ was detected within a 110 ℃ PFA resonator cavity. NO was injected to destroy $NO_3$ from $N_2O_5$ thermal decomposition every 5 min cycle, and the result was used as the reference spectrum to avoid the influence of ambient water vapor. A pair of high-reflectivity (HR) mirrors (Layertec GmbH, Mellingen, Germany) with a diameter of 25.0 mm (C0.00/-0.10 mm) was used to enhance the effective optical pathlength. Mirror reflectivity (R(λ)) was calibrated with high purity He and $N_2$ in the current experimental setup during the field measurements. R(λ) was calibrated to be 0.99997, and the effective pathlength of the optical resonator was 13.96 km. A Teflon polytetrafluoroethylene (PTFE) filter was used to remove ambient aerosol particles, and the inlet flow rate was 1.0 $L \cdot min^{-1}$. The loss of $N_2O_5$ in the sampling line and filter was considered in the data correction according to previous work (Wang et al., 2017a). Here the CEAS measurement encompasses the combined concentration of ambient [$N_2O_5$ + $NO_3$] and effectively represents $N_2O_5$ under high $NO_x$ (or low temperature) conditions when the $NO_3$-to-$N_2O_5$ ratio is likely to be low. Accounting for the instrument's transmission efficiency and the thermal transformation between $NO_3$ and $N_2O_5$, the contribution of $NO_3$ is sufficiently negligible in comparison to $N_2O_5$. Nevertheless, we have taken it into account during the $N_2O_5$ data correction. The limit of detection (LOD) was 2.7 pptv (1σ), and the measurement uncertainty was ± 19%.

**Table 1.** The information of observation instruments used during the DWS campaign.

| Species | Techniques | Detection limit | Accuracy | Time resolution |
|---|---|---|---|---|
| $N_2O_5$ | CEAS | 2.7 pptv (1σ) | ±19% | 10 s |
| NO | Chemiluminescence | 0.4 ppbv | ±5% | 1 min |

| | | | | |
|---|---|---|---|---|
| $NO_2$ | Chemiluminescence | 0.4 ppbv | ±5% | 1 min |
| $O_3$ | UV photometry | 0.4 ppbv | ±5% | 1 min |
| VOCs | PTR-TOF-MS | 0.01 ppbv | ±10% | 10 s |
| PNSD | SMPS | 5–300 nm | ±10% | 5 min |

$NO_x$ and $O_3$ were measured by commercial instruments (model T200U and model T400U, Teledyne API Inc., respectively) calibrated with zero air before the measurement. The nitrogen oxide analyzer uses the chemiluminescence detection method to measure the original NO and converted $NO_2$, and the LOD was 0.4 ppbv for each species. Aerosol surface area density ($S_a$, $\mu m^2$ $cm^{-3}$) was calculated based on the particle numbers and geometric diameter, which was calculated through the results measured by a laboratory-assembled scanning-mobility particle sizer (SMPS) according to Mcmurry et al. (2000). This SMPS system consists of two differential mobility analyzers (DMA, "nano-DMA" mode 3081A, and "regular-DMA" mode 3085A, TSI Inc.) in parallel, and a condensed particle counter (mode 3787, TSI Inc.) as the detector. The combination of nano DMA and conventional mode 3085A DMA enables the SMPS to have better detection performance for particles below 50 nm. In this measurement, SMPS measured the particle size distribution in 5-300 nm with a time resolution of 5 minutes, and $S_a$ can be regarded as the lower limit value. A growth factor $f(RH) = 1 + 8.8 \times (RH/100)^{9.7}$ (Liu et al., 2013) was used here to correct dry state $S_a$ to wet state $S_a$.

VOCs were measured by proton transfer reaction time of flight mass spectrometry (PTR-TOF-MS, Ionicon Analytik GmbH, Innsbruck, Austria) with a time resolution of 10 s. At the end of this campaign, background measurements and instrument calibration were conducted with high-purity nitrogen and multi-component VOC gas standards, respectively. The instrument calibration results yielded strong linear relationships ($R^2 = 0.98$) between the proton transfer reaction rate constants and the sensitivities of ten calibrants, including acetaldehyde, acetone, dimethyl sulfide, isoprene, methyl ethyl ketone, benzene, toluene, styrene, o-xylene, and trimethylbenzene. The sensitivities of the uncalibrated species were determined through the rate constants of the proton transfer reactions and their correlation coefficients with sensitivity. Meanwhile, the VOCs were also sampled by canister and analyzed by a gas chromatograph equipped with a mass spectrometer or flame ionization detector (GC-MS) for some ozone-polluted days. For the absence of nocturnal data from canister samples, the following analysis was based on the PTR-TOF-MS measurement except the weight of α-pinene and β-pinene detected by GC-MS. Since monoterpene species cannot be distinguished by PTR-TOF-MS, the reaction rate constant of the sum monoterpene reaction with $NO_3$ was weighted by the campaign-averaged weight of α-pinene and β-pinene detected by GC-MS. Meteorological parameters (i.e., temperature (T), relative humidity (RH), wind speed, and wind direction) were routinely monitored with a time resolution of 5 min.

## 2.3 The calculation of $NO_3$ budget and lifetime

With the observation of $N_2O_5$, $NO_3$ can be calculated according to their temperature-dependent equilibrium relationship (Eq. 1) (Brown and Stutz, 2012). Lifetimes are commonly expressed as the ratio of their concentrations to the $NO_3$ production rate as determined by Eq. 2 and Eq. 3, assuming the production and loss are in dynamic balance at night (Brown et al., 2003; Brown and Stutz, 2012). The production rate of nitrate radical, $P(NO_3)$, is commonly expressed by Eq. 4, where $k_{NO_2+O_3}$ represents the temperature-dependent reaction rate constant of $NO_2$ and $O_3$ (Atkinson et al., 2004). In general, the nocturnal $NO_3$ losses typically include three main pathways (Eq. 5): (1) the reaction with NO, (2) the reactions with VOCs, and (3) $N_2O_5$ uptake.

$$[NO_3] = [N_2O_5]/\mathrm{Keq}(T)[NO_2]$$

$$\mathrm{Keq} = 5.50 \times 10^{-27} \times \exp(10724/T) \quad \text{(Eq. 1)}$$

$$\tau_{N_2O_5} = \frac{[N_2O_5]}{P(NO_3)} = \frac{[N_2O_5]}{k_{NO_2+O_3}[NO_2][O_3]} \quad \text{(Eq. 2)}$$

$$\tau_{NO_3} = \frac{[NO_3]}{P(NO_3)} = \frac{[NO_3]}{k_{NO_2+O_3}[NO_2][O_3]} \quad \text{(Eq. 3)}$$

$$P(NO_3) = k_{NO_2+O_3}[O_3][NO_2] \quad \text{(Eq. 4)}$$

$$L(NO_3) = \sum k_i[VOC_i][NO_3] + k_{NO+NO_3}[NO][NO_3] + k_{het}[N_2O_5] \quad \text{(Eq. 5)}$$

The $NO_3$ reactivity towards VOCs, $k(NO_3)$, is the first-order loss rate coefficient calculated from the products of the bimolecular rate coefficients $k_i$ and the VOC concentrations as shown in Eq. 6.

$$k(NO_3) = \sum k_i[VOC_i] \quad \text{(Eq. 6)}$$

The $k_{het}$ is the first-order loss rate coefficient of $N_2O_5$ uptake on the aerosol surface. It depends on the uptake coefficient $\gamma(N_2O_5)$, the aerosol surface area density $S_a$ ($\mu m^2\ cm^{-3}$), and the mean molecular speed $c$ (Eq. 7). The $\gamma(N_2O_5)$ is influenced by chemical composition, physical properties of aerosol, as well as ambient conditions including related humidity and temperature (Yu et al., 2020; Wagner et al., 2013; Wang et al., 2018b; Bertram and Thornton, 2009; Tang et al., 2014; Kane et al., 2001). There are several kinds of methods proposed to quantify or estimate $\gamma(N_2O_5)$ by using observed parameters. Given

that some essential parameters were not directly measured during this campaign, only two approaches were employed to estimate the $N_2O_5$ uptake coefficient. The first method is the pseudo steady state method by assuming that $N_2O_5$ and $NO_3$ have achieved a steady state (Brown et al., 2009). $\gamma(N_2O_5)$ and $k_{NO_3}$ can be determined from the slope and intercept of linear regression of $K_{eq}[NO_2]\,\tau(N_2O_5)^{-1}$ versus $0.25cS_aK_{eq}[NO_2]$ respectively as shown in Eq. 8. The second is the parameterization method. As the aerosol compositions used to estimate the $N_2O_5$ uptake coefficients were not measured, only a simplified parameterization is available that based on relative humidity (RH) and temperature (Eq. 9) (Hallquist et al., 2003; Kane et al., 2001; Evans and Jacob, 2005). Although simple, it had an overall reasonable performance in China (Wang et al., 2022; Tham et al., 2018; Wang et al., 2020a).

$$k_{het} = \frac{1}{4}cS_a\gamma(N_2O_5) \qquad \text{(Eq. 7)}$$

$$K_{eq}[NO_2]\tau(N_2O_5)^{-1} = \frac{1}{4}cS_a\gamma(N_2O_5)K_{eq}[NO_2] + k_{NO_3} \qquad \text{(Eq. 8)}$$

$$\gamma(N_2O_5) = \alpha \times 10^{\beta}$$

$$\alpha = 2.79 \times 10^{-4} + 1.3 \times 10^{-4} \times RH - 3.43 \times 10^{-6} \times RH^2 + 7.52 \times 10^{-8} \times RH^3$$

$$\beta = 4 \times 10^{-2} \times (T - 294) \ \ (T > 282K)$$

$$\beta = -0.48 \ \ (T < 282K) \qquad \text{(Eq. 9)}$$

## 3. Results and discussion

### 3.1 Measurement overview

The time series of $N_2O_5$, related trace gases, and selected meteorological parameters for the study period are depicted in Fig. 2. The air masses are categorized into IAM and CAM according to the backward trajectories at 20:00, 00:00, and 04:00 each day as illustrated in Fig. 1. The detailed information of two kinds of air masses is listed in Table 2. Data gaps for $N_2O_5$ were caused by technical problems, mirror reflectivity calibration, or instrumental maintenance, which usually took place in the daytime. In this campaign, meteorological conditions featured a typical subtropical winter climate with average temperature and RH values of 20.1 ± 1.9 ℃ and 52.0% ± 13.6%, respectively.

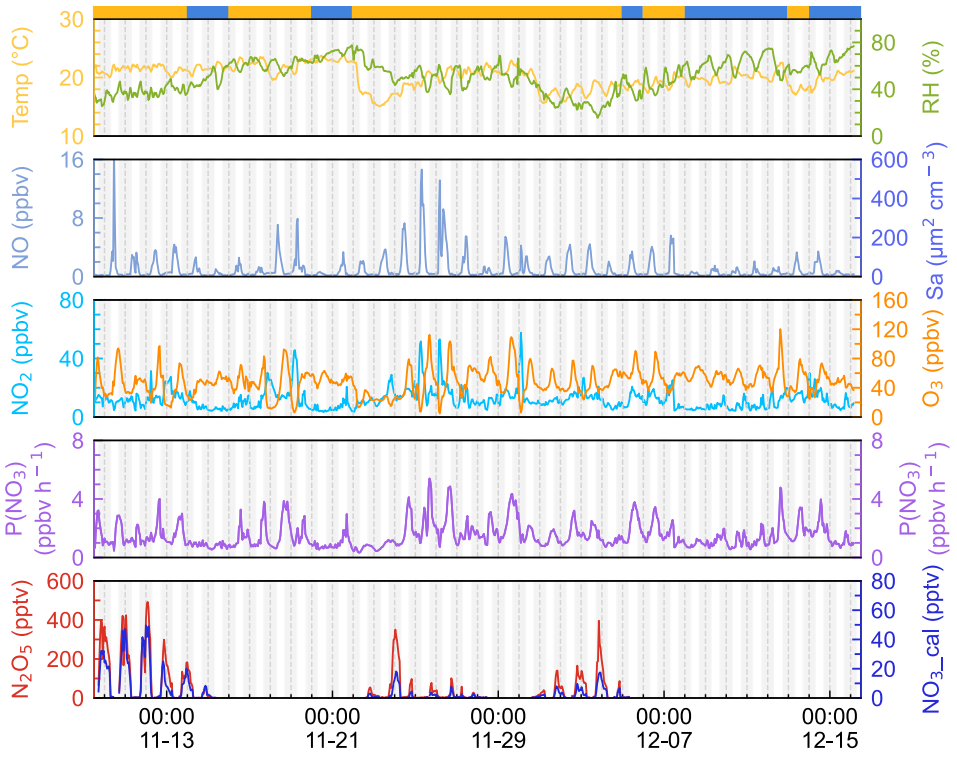


**Figure 2.** Time series of $N_2O_5$, $NO_3$, $P(NO_3)$, NO, $NO_2$, $S_a$, temperature, and relative humidity in 1-hour average. $NO_3$ was calculated by measured $N_2O_5$ according to the thermal equilibrium. The light gray shadow indicates the nighttime period. The ribbon at the top separates the air masses into two categories, yellow for IAM and blue for CAM.

Ozone exhibited the characteristic of afternoon photochemical peaks especially when the airmass comes from the inland. The average and maximum concentrations of ozone were 48.2 ± 18.2 ppbv and 120.1 ppbv, respectively. Once the maximum hourly average $O_3$ exceeded the Chinese national air quality standard (200 μg $m^{-3}$, equivalent to 93 ppbv), we marked this day as an $O_3$ pollution day. There are 6 $O_3$ polluted days out of 37 days during the campaign and all occurred during IAM periods. Meanwhile, the mixing ratio of NO, $NO_2$, and $S_a$ usually increased during these days, indicating that this site was strongly affected by regional transport from the PRD city clusters. Previous observations by Wang et al. (2018a) also found high $O_3$ levels in autumn on the same island due to the weak NO titration and high $O_3$ production rate.

Nitrogen oxides ($NO_x$ = NO + $NO_2$) were at a moderate level with an average value of 13.1 ± 8.2 ppbv, which is much lower than the values in PRD regions (usually > 20 ppbv, (Wang et al., 2022; Yang et al., 2022; Yun et al., 2018b) and higher than those on the remote islands in South China Sea (< 5 ppbv, Chuang et al., 2013). The mixing ratio of NO at nighttime was low and showed small peaks during daytime. With the $O_3$ accumulating throughout the day, NO decreased to below the instrument detection limit in the first half of the night,

while it began to increase as the $O_3$ concentration decreased in the second half of the night. Given that the lifetime of NO is only a few minutes in the presence of several tens of ppbv of $O_3$ (Dewald et al., 2022), we inferred that NO is likely originating from a local source such as soil emission, boats, cooking, and so on.

**Table 2.** Summary of parameters on the two air mass types (mean ± standard deviation).

| Species | IAM | | CAM | |
|---|---|---|---|---|
| | All day [b] | Nighttime [b] | All day | Nighttime |
| $O_3$ (ppbv) | 45.8 ± 20.2 | 42.9 ± 18.4 | 53.1 ± 11.9 | 51.4 ± 9.6 |
| $NO_x$ (ppbv) | 15.1 ± 8.7 | 14.5 ± 9 | 9.2 ± 5.1 | 8.8 ± 4.8 |
| $NO_2$ (ppbv) | 13.9 ± 7.6 | 14.1 ± 8.3 | 8.6 ± 4.8 | 8.6 ± 4.8 |
| NO (ppbv) | 1.2 ± 2.3 | 0.4 ± 1.1 | 0.5 ± 0.6 | 0.2 ± 0.1 |
| Temp (°C) | 19.9 ± 2 | 19.9 ± 1.9 | 20.8 ± 1.5 | 20.6 ± 1.5 |
| RH (%) | 46.7 ± 12.5 | 47.7 ± 13.2 | 61.2 ± 10 | 64.1 ± 9.6 |
| $P(NO_3)$ (ppbv $h^{-1}$) | 1.6 ± 0.9 | 1.5 ± 0.8 | 1.3 ± 0.8 | 1.2 ± 0.6 |
| $N_2O_5$ (pptv) | - [c] | 119.5 ± 128.6 | - [c] | - |
| $NO_3$ (pptv)[a] | - | 9.9 ± 12.5 | - | - |
| $\tau_{N_2O_5}$ (min) | - | 6.5 ± 6.5 | - | - |
| $\tau_{NO_3}$ (min) | - | 0.5 ± 0.7 | - | - |

Note: [a] $NO_3$ is calculated by the thermal equilibrium between $NO_2$, $NO_3$, and $N_2O_5$.
[b] "All day" means the 24-hour average and the "Nighttime" means the time between 18:00-06:00 local time.
[c] Without $N_2O_5$ measurement in the daytime and limited $N_2O_5$ data during the CAM period, $N_2O_5$, $NO_3$, and their lifetimes were not valid here.

$N_2O_5$ was at a moderate level on most days with a nocturnal average of 119.5 ± 128.6 pptv, with high concentrations (>400 pptv in 1-hour average) in the first three days during this campaign. During the nights from November 9$^{th}$ to 12$^{th}$, the $N_2O_5$ concentrations were significantly higher than those on other nights, with a maximum of 657.3 pptv at midnight of November 12$^{th}$. The $NO_3$ concentration (calculated based on the thermal equilibrium with $N_2O_5$) was also moderate with an average mixing ratio of 9.9 ± 12.5 pptv, which was higher than that reported on a nearby coastal site of Hong Kong Island (Yan et al., 2019). Table 3 compares the $N_2O_5$, $NO_3$, and $P(NO_3)$ found in other coastal (or island) and continental regions from Europe, the United States, and China. In our study, $N_2O_5$ and $NO_3$ were at a moderate level compared to other coastal regions when they were affected by emission plumes from continental regions, such as Northwestern Europe (Morgan et al., 2015), the East coast of the USA (Brown et al., 2004), and Shenzhen, China (Niu et al., 2022), and were comparable with urban regions (Wang et al., 2017b; Wang et al., 2018b).

The concentrations of $NO_3$ precursors ($NO_2$ and $O_3$) at this site were much similar to some rural areas, leading to a high $NO_3$ production rate with a daily average of 1.5 ± 0.9 ppbv $h^{-1}$ and a maximum of 5.9 ppbv $h^{-1}$. The average value is much higher than that reported in Beijing in winter (0.4 ppbv $h^{-1}$, Wang et al., 2021), comparable to autumn (1.4 ± 1.7 ppbv $h^{-1}$, Wang et al., 2017b) and even higher than that in summer Taizhou (1.01 ± 0.47 ppbv $h^{-1}$, Wang et al., 2020a). The nocturnal average $P(NO_3)$ during this campaign was 1.4 ± 0.7 ppbv $h^{-1}$, which is higher than the average value in the warm season of China with 1.07 ± 0.38 ppbv $h^{-1}$ (Wang et al., 2023). The high reaction rate constant for $NO_2$ and $O_3$ due to the high temperature at this site is a potential explanation for the high $P(NO_3)$ values observed in this study (i.e., at the same $NO_2$ and $O_3$ level, if the temperature increased from 10 ℃ to 20 ℃, the reaction rate constant would increase from $2.27\times10^{-17}$ to $3.05\times10^{-17}$, which means the $P(NO_3)$ would be 1.34 times faster). The high $P(NO_3)$ and the low concentrations of $N_2O_5$ and $NO_3$ indicate intensive atmospheric oxidation capacity and fast $NO_3$ and $N_2O_5$ removal over the Pearl River Estuary.

The mean diurnal profiles of $N_2O_5$, together with relevant species are shown in Fig. 3. Daytime $N_2O_5$ and $NO_3$ in the IAM period were shown as NaN due to the absence of observation. Because of limited $N_2O_5$ data for the CAM period, neither $N_2O_5$ nor $NO_3$ is shown in Fig. 3. NO exhibited similar diurnal variation in both periods and the mixing ratio was higher in the IAM period. The wind rose plot (Fig. S1) showed high concentrations of NO originating from the north characterized by the outflow from PRD regions. However, $NO_2$ differed in the two periods, showing high anti-correlation with $O_3$ only in the IAM period and little diurnal variation in the CAM period.

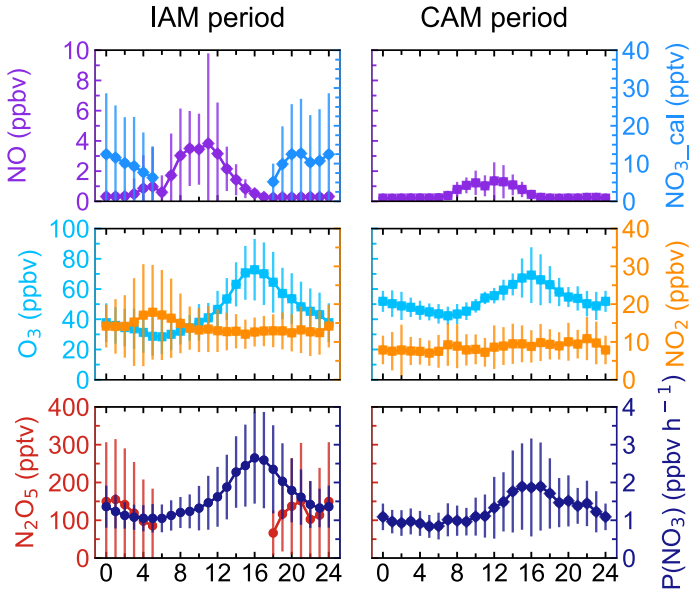


**Figure 3.** Mean diurnal profiles of $N_2O_5$, $NO_3$, $P(NO_3)$, and relevant parameters in the two

types of air masses. $NO_3$ was calculated from $N_2O_5$. Neither $N_2O_5$ nor $NO_3$ was shown during the CAM period because of limited $N_2O_5$ measurement.

Ozone exhibited a typical diurnal pattern for all air masses, gradually increasing until its peak at 16:00 and then slowly decreasing throughout the night until its lowest mixing ratio was reached at about 06:00. Compared to the CAM period, the lower minimum hourly $O_3$ concentration and a small peak of $NO_2$ in the early morning indicated that NO titration effect was stronger in the IAM period, and the higher maximum of $O_3$ concentration in IAM indicated that photochemical formation of $O_3$ and/or transport was faster to completely offset the titration. In addition, the higher $NO_x$ and VOC concentrations (as shown in Table S1) in the IAM period facilitated $O_3$ formation. With the elevated precursor concentrations ($NO_2$ and $O_3$) in the IAM period, $N_2O_5$ and $NO_3$ accumulated rapidly after sunset, reaching their peak values (492.1 pptv and 49.6 pptv for each). $P(NO_3)$ was highly consistent with $O_3$ in diurnal variation and reached the peak at 16:00, with peak values of 2.7 ppbv $h^{-1}$ (IAM) and 1.9 ppbv $h^{-1}$ (CAM), as well as a nocturnal average value of 1.5 ± 0.8 ppbv $h^{-1}$ (IAM) and 1.2 ± 0.6 ppbv $h^{-1}$ (CAM), respectively. The $P(NO_3)$ of CAM was consistent with the observation when the air mass over eastern Shenzhen was transported from the clean area or sea surface (1.2 ± 0.3 ppbv $h^{-1}$, Niu et al., 2022).

**Table 3.** Summary of field-observed $N_2O_5$, $NO_2$, $O_3$ concentrations, and $NO_3$ production rate.

| Region | Location | Time | $N_2O_5$ (pptv) | $NO_3$ (pptv) | $NO_2$ (ppbv) | $O_3$ (ppbv) | $P$ ($NO_3$) (ppbv $hr^{-1}$) | References |
|---|---|---|---|---|---|---|---|---|
| Urban | Jinan, China | Aug.-Sep.,2014 | 22 ± 13 (max 278) | / | 74.6 | 55 | / | (Wang et al., 2017c) |
| Urban | Shanghai, China | Aug.-Oct., 2011 | 310 ± 380 | 16±9 (max 95) | 0-76 | 23 ± 8 (max 57) | 1.10 ± 1.09 | (Wang et al., 2013) |
| Urban | Beijing, China | May-Jul., 2016 | 100–500 (max 937) | 27 | / | / | 1.2 ± 0.9 | (Wang et al., 2018b) |
| Urban | Mt. Tai, China | Jul.-Aug., 2014 | 6.8±7.7 | / | 16.4 (±6.1) | 88.6 (±16.6) | 0.45±0.40 | (Wang et al., 2017d) |
| Urban | Heshan, China | Sep.-Nov., 2019 | 64 ± 145 (night) | max 90 | 21.0±10.4 | 75.2±20.9 (max 152.8) | 2.5 ± 2.1 (day) | (Wang et al., 2022) |
| | | | (max 1180) | | | | 1.8 ±1.5 (night) | |
| Urban | Beijing, China | Sep.-Oct., 2019 | 68.0 ±136.7 | / | 35.1 ±16.6 | 27.7 ±25.2 | 2.25 ±2.02 | (Wang et al., 2017b) |
| Suburban | Changzhou, China | May-Jul., 2019 | 53.4 ± 66.1 (max 304.7) | 4.7 ± 3.5 (max 17.7) | 13.7 ± 8.9 | 48.4 ± 27.8 | 1.7 ± 1.2 (max 7.7) | (Lin et al., 2022) |
| Rural | Wangdu, China | Jun.-Jul., 2014 | <200 (max 430) | / | 10-80 | (max 146) | 1.7 ±0.6 | (Tham et al., 2016) |
| Rural | Taizhou, China | May-Jul., 2018 | 26.0 ± 35.7 (max 492) | 4.4 ± 2.2 (max 150) | 28.28 ± 18.57 | 48.2 ± 32.5 | 1.01 ± 0.47 (night) | (Wang et al., 2020a) |
| Coastal | Tai Mo Shan, HK | Nov.-Dec., 2013 | 0.5-11.8 ppbv | / | 7.88 | 68.5 | 0.01-2 | (Brown et al., 2016) |
| Coastal | East Coast of USA | Jun.-Aug., 2002 | 85 | 17 | 6 | 35 | / | (Brown et al., 2004) |
| Coastal | California, USA | Jan.,2004 | 0-200 | / | 0-15 | 15–35 | / | (Wood et al., 2005) |
| Coastal | Southern Spanish | Nov.-Dec., 2018 | ~500 (max) | / | 1-15 | 15-40 | / | (Crowley et al., 2011) |
| Coastal | Shenzhen, China | Sep.-Oct., 2019 | 55.6 ± 89 (max 1420) | / | 6.2 | 88.9±24.6 | 2.9 ± 0.5 (UAM) | (Niu et al., 2022) |
| | | | 45.4 ± 55.2 (BAM) | | | | 1.2 ± 0.3 (BAM) | |
| Coastal | Northwestern Europe | Jul., 2010 | 670 | / | 0.5–2 | 30– 40 | / | (Morgan et al., 2015) |
| Island | Hok Tsui, HK | Aug.-Sep., 2012 | 17±33 (max 336) | 7 ± 12 | 6 ± 7 | 33 ± 24 | / | (Yan et al., 2019) |
| Island | Wanshan, China | Nov.-Dec., 2021 | 107.22 ± 125.17 | 7.56 ± 10.95 | 13.14 ± 8.68 | 43.75 ± 18.49 | 1.38 ± 0.83 | This work |

Notes: UAM means air masses coming from continental areas, and BAM means air masses coming from background marine areas. Mean values are in the form of mean ± standard deviation or single data. The maximum was noted in the table.

### 3.2 The lifetimes of $N_2O_5$ and $NO_3$

Steady-state lifetime is one of the most common and useful diagnostics for $NO_3$ and $N_2O_5$ analysis in the atmosphere (Brown et al., 2003; Wang et al., 2018b; Wang et al., 2020a; Brown et al., 2016). As shown in Fig. 4, $\tau_{NO_3}$ was low during the whole campaign with an average of 0.5 ± 0.7 min. $\tau_{N_2O_5}$ showed a similar pattern to $\tau_{NO_3}$ but had a much higher value, ranging from 0 to 34.1 min with an average of 6.1 ± 6.5 min. The $N_2O_5$ lifetime was higher in the first half of the campaign (11.5 min, November 9$^{th}$ to 14$^{th}$) than in the second half (3.5 min, November 22$^{th}$ to 28$^{th}$). The difference was mainly due to the $N_2O_5$ mixing ratio rather than $P(NO_3)$, as $P(NO_3)$ shows no significant difference during the whole observation (Fig. 2).

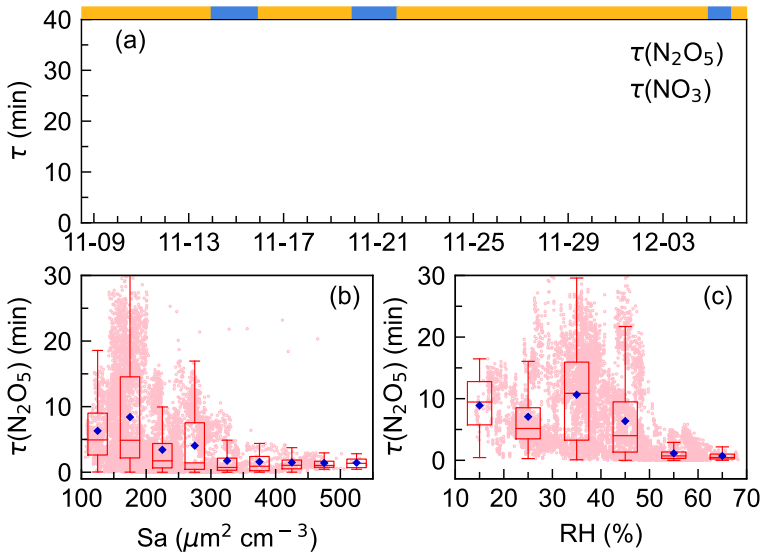


**Figure 4.** Time series of $N_2O_5$ and $NO_3$ lifetimes (a) and variations of nocturnal $N_2O_5$ lifetime as a function of aerosol surface area density, $S_a$ (b), and relative humidity, RH (c). The blue diamond represents the average $\tau_{N_2O_5}$ and pink dots represent the scatter data point in 1 min. The ribbon at the top separates the air masses into two categories, yellow for IAM and blue for CAM.

$\tau_{N_2O_5}$ values were comparable to those measured on the coastline of Finokalia, Greece for a median of 5 min (Vrekoussis et al., 2004; Vrekoussis et al., 2007), but much lower than those previously reported in the residual layer in Hong Kong for 1-5 h (Brown et al., 2016). In comparison, the lifetimes were much longer than in inland urban areas, for example, 0.93 ± 1.13 min in Taizhou (Li et al., 2020), 1.6 ± 1.5 min in Changzhou (Lin et al., 2022) for YRD regions, 1.1-10.7 min (Zhou et al., 2018) and 4.5 ± 4.0 min (Wang et al., 2018b) in Beijing. Typically, high aerosol loading, more intensive VOC, and NO emissions in these

areas led to enhanced $N_2O_5$ uptake and reactions of $NO_3$ with VOC. While in this site, measurement indicated that the peak diameter in the particle number distribution was small during the whole campaign and indicated no significant difference between the two air masses with respect to the aerosol diameters (Fig. S2). $S_a$ value ranged from 29 $\mu m^2$ $cm^{-3}$ to 557 $\mu m^2$ $cm^{-3}$. All of these indicated the atmosphere was relatively clean (Wang et al., 2017b), making $N_2O_5$ uptake slow. Fig. 4b shows $N_2O_5$ lifetime decreased rapidly from 8.3 min to 1.7 min when $S_a$ increased up to 300 $\mu m^2$ $cm^{-3}$ and then remained at relatively low constant levels though $S_a$ still increased. Such a trend of $\tau_{N_2O_5}$- $S_a$ dependence was consistent with previous observations and varied in exact values (Zhou et al., 2018; Wang et al., 2018b; Li et al., 2020). Fig. 4c showed that $\tau_{N_2O_5}$ decreased as RH increased ( > 40%) possibly due to the hygroscopic aerosol growth and the dependence of the $N_2O_5$ uptake coefficient on the RH (Brown and Stutz, 2012). Overall, the trend is consistent with previous works, while the large discrepancy of the dependence implied that $N_2O_5$ uptake was not the dominant $NO_3$ loss process.

### 3.3 The $NO_3$ reactivity and $N_2O_5$ uptake coefficients

The concurrent high $P(NO_3)$ and low $NO_3$ lifetime imply high $NO_3$ reactivity as well as a large nocturnal $NO_3$ loss process at DWS. The $NO_3$ reactivity towards VOCs was calculated by Eq. 4, towards which were categorized into anthropogenic VOC and biogenic VOC (Gu et al., 2021). Throughout the campaign, $k(NO_3)$ varied considerably (Fig. 5a), showing relatively high and fluctuated values when the airmasses featured IAM. The $k(NO_3)$ ranged from $1.6\times10^{-3}$ $s^{-1}$ to $2.4\times10^{-2}$ $s^{-1}$ with the daily average of $4.6 \pm 2.8\times10^{-3}$ $s^{-1}$. Low values of $k(NO_3)$ were observed from December 9$^{th}$ to 12$^{th}$ when the air masses originate from coastal or offshore from the east and southeast, which features the outflow of coastal cities like Hong Kong and Shenzhen.

Fig. 5b shows the mean diurnal profile of $k(NO_3)$, where a trend of high values in the daytime and low values at nighttime are observed. Anthropogenic VOC, especially cresol, dominated the daily trend of $k(NO_3)$, while biogenic VOC-$k(NO_3)$ showed no significant diurnal variation. Except cresol, other highly reactive VOC showed little change throughout the day. Regarding the biogenic VOC-$k(NO_3)$, the concentrations of monoterpene, isoprene, and DMS changed smoothly although their emissions would increase with elevated temperature and sunlight during daytime (Fuentes. et al., 2000). The detailed contributions of VOC categories to $k(NO_3)$ were shown in Fig. 5c. The $k(NO_3)$ was $5.6 \pm 2.8\times10^{-3}$ $s^{-1}$ and $3.7 \pm 2.5\times10^{-3}$ $s^{-1}$ on average for daytime and nighttime, respectively. The daytime distribution of $k(NO_3)$ differed from that at the mountaintop of Tai Mo Shan in Hong Kong (Brown et al., 2016). During the nighttime, anthropogenic VOC-$k(NO_3)$ tripled the biogenic VOC-$k(NO_3)$ and was dominated by cresol (26.4%). The

nighttime k($NO_3$) corresponded to a $NO_3$ lifetime of 4.5 min, which was about 10 times the lifetime derived from steady-state analysis, indicating that the reaction of $NO_3$ with VOC was not significant enough. The faster $NO_3$ loss rate also indicated the less aged air mass that was influenced by surface-level emissions.

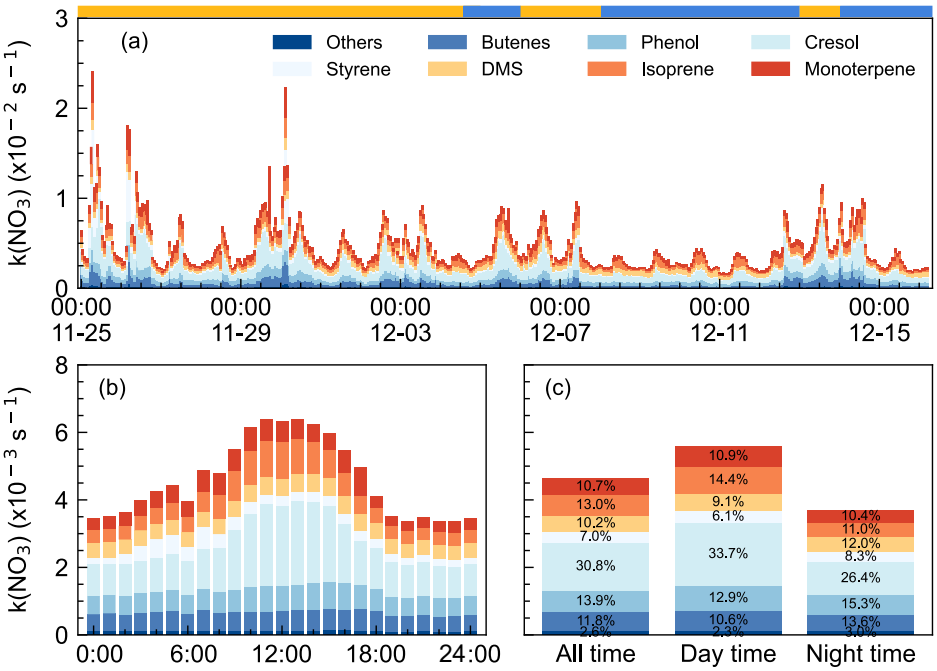


**Figure 5.** $NO_3$ reactivity via VOCs during the campaign. (a) k($NO_3$) time series from Nov. 25th to Dec. 15th; (b) mean diurnal profiles; and (c) the relative contribution in different categories. The ribbon at the top separates the air masses into two air masses types, yellow for IAM and blue for CAM.

We showed that $NO_3$ reactivity and its composition in this study exhibited significant differences compared to other urban or forested regions (Wang et al., 2017d; Ayres et al., 2015; Brown et al., 2016; Lin et al., 2022). Although anthropogenic VOCs played a dominant role, accounting for 66.1%, the major contributors were not low-carbon alkenes but phenol (13.9%, 0.64 ± 0.28 $\times 10^{-3}$ $s^{-1}$) and cresol (30.8%, 1.4 ± 1.0 $\times 10^{-3}$ $s^{-1}$), which have received little attention in previous studies. Despite their relatively low concentrations, averaging 7 ± 3 pptv and 4 ± 3 pptv respectively, their substantial contribution to k($NO_3$) is notable due to their fast rate constants ($3.8 \times 10^{-12}$ $cm^3$ $molecule^{-1}$ $s^{-2}$ and $1.4 \times 10^{-11}$ $cm^3$ $molecule^{-1}$ $s^{-2}$ at 298 K, respectively) for reaction with $NO_3$. Considering that the measured phenol and cresol concentration is low and near the instrumental detection limit, we note this may bring some uncertainties in quantifying the contribution to the total $NO_3$ reactivity and $NO_3$ loss rate. These substances are mainly secondary species from aromatic

compounds and higher concentrations have also been observed, such as in the Strasbourg area, France (14 pptv, Delhomme et al., 2010) and in Great Dun Fell, UK (16 pptv, Lüttke et al., 1997). Hence, these phenolic compounds were potentially important but often overlooked for their contributions to $NO_3$ reactivity in urban areas, and their reactions with $NO_3$ may also contribute to the formation of nitrophenol. These reactions warrant further attention in future research. Regarding biogenic VOCs, besides the contributors commonly observed in forest regions such as monoterpenes and isoprene, the marine emissions indicator, dimethyl sulfide (DMS), contributed 10.2% to $NO_3$ reactivity (daily average). Previous studies have suggested that DMS may serve as a major direct sink for $NO_3$ in clean marine regions (Allan et al., 1999; Aldener et al., 2006; Brown et al., 2007). However, this study reveals that anthropogenic VOC emissions significantly enhanced the $NO_3$ reactivity in marine areas, highlighting the crucial influence of anthropogenic activities on marine atmospheric chemistry.

As shown in Fig. 6a, $k(NO_3)$ differed significantly between the inland and coastal air masses, with $5.2 \pm 3.1\times10^{-3}$ $s^{-1}$ and $3.7 \pm 1.9\times10^{-3}$ $s^{-1}$ on average in IAM and CAM periods, respectively. Of which anthropogenic VOC-$k(NO_3)$ in IAM ($3.5 \pm 2.3\times10^{-3}$ $s^{-1}$) was higher than in CAM ($2.3 \pm 1.4\times10^{-3}$ $s^{-1}$) and dominant in both air masses, while biogenic VOC-$k(NO_3)$ was comparable ($1.7 \pm 0.9 \times10^{-3}$ $s^{-1}$ and $1.4 \pm 0.6\times10^{-3}$ $s^{-1}$ for IAM and CAM, respectively). The difference indicated that this region was affected by long-range transport emissions to a certain extent. The pie charts in Fig. 6b showed different VOC categories that contributed to $k(NO_3)$ in two periods with AVOC dominant at any time. The change in the relative contribution of various VOCs to $k(NO_3)$ varied simultaneously throughout the day, showing an increase in butene, phenol, and DMS, and a decrease in cresol and monoterpene from daytime to nighttime.

$N_2O_5$ heterogeneous uptake on aerosol is one of the vital loss processes of $NO_3$ and the uptake coefficient varied greatly under different environmental conditions. For instance, $\gamma(N_2O_5)$ can reach up to 0.072 in polluted urban regions (Wang et al., 2017b; Wang et al., 2018b; Lu et al., 2022; Li et al., 2020), while usually below 0.03 in coastal areas (Brown et al., 2016; Morgan et al., 2015; Niu et al., 2022). $N_2O_5$ uptake coefficient can be gotten from the pseudo steady state method by assuming that $N_2O_5$ and $NO_3$ have achieved a steady state (Brown et al., 2009), in which the fitted slope represents $\gamma(N_2O_5)$ and the intercept represents the direct loss rate coefficient, $k(NO_3)$ (as shown in Eq. 8). However, this approach failed to generate valid results in our study since a negative slope or intercept was observed (Fig. S4). These results indicated that a large $NO_3$ removal process existed at this site, making it unable to approach a stable state. The $\gamma(N_2O_5)$ was also calculated from Nov. 9$^{th}$ to 16$^{th}$ by using the simplified parameterization, as shown in Eq. 9. The parameterized average $\gamma(N_2O_5)$ showed a large variation ranging from 0.0014 to 0.0299,

with an average of 0.0095 ± 0.0059. This value is within the range from <0.0016 to 0.03 derived from the ambient observation around other coastal areas (Niu et al., 2022; Yun et al., 2018a; Brown et al., 2006; Brown et al., 2016; Morgan et al., 2015) and smaller than the polluted North China Plain (Wang et al., 2017c; Wang et al., 2017b; Wang et al., 2017d; Tham et al., 2018).

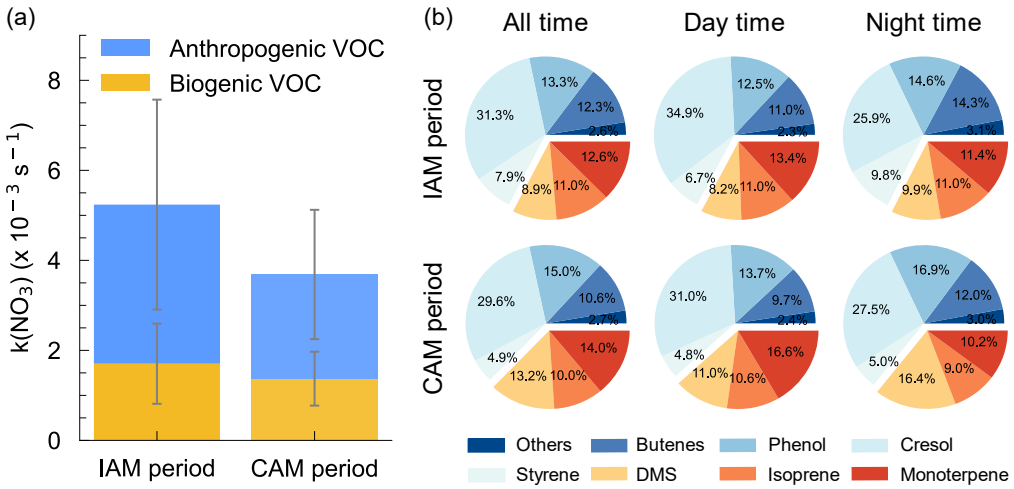


**Figure 6.** (a) Distributions of k($NO_3$) from AVOC and BVOC for both IAM and CAM periods. The error bar indicates the standard deviation. (b) The relative contribution of VOC categories to the k($NO_3$).

### 3.4 The $NO_3$ loss budget

To assess the contribution of various loss processes to the total $NO_3$ removal, we calculated their loss rate and the loss ratio, *LR*($NO_3$). The *LR*($NO_3$) is defined as the sum of the loss rate by process X (VOC or $N_2O_5$ uptake) to the total $NO_3$ loss rate, here the total $NO_3$ loss rate is represented by P($NO_3$) since we cannot quantify the total $NO_3$ loss rate due to the NO concentration below the limit of instrument detection. Due to the data absence of measured VOCs or $N_2O_5$ during certain periods, the loss proportion of VOCs and $N_2O_5$ uptake in $NO_3$ loss only presented from Nov. 26$^{th}$ to Dec. 5$^{th}$ during which all air masses originated from continental China. As shown in Fig. 7, a closer examination revealed that the nights can be divided into two periods, period I: November 25$^{th}$ to 28$^{th}$ when the loss ratio of VOC and $N_2O_5$ uptake remained below 3%, and period II: November 30 to December 4 when the loss ratio was higher. Both periods had large nocturnal $NO_3$ production rates with an average of 2.1 ± 1.1 ppbv h$^{-1}$ in period I and 1.4 ± 0.6 ppbv h$^{-1}$ in period II, respectively.

$N_2O_5$ uptake rate was larger in period I (0.01 ± 0.01 ppbv $h^{-1}$) than that in period II (0.006 ± 0.004 ppbv $h^{-1}$), which can be explained by the increased RH, $S_a$, and $N_2O_5$ concentration as shown in Fig. 2. The loss ratio of these processes was shown in Fig. 7b, the total $NO_3$ loss through reactions with VOCs and $N_2O_5$ uptake accounted for less than 20%, with an average of 1.2% (period I) and 5.3% (period II), respectively. This result shows that the nighttime $NO_3$ chemistry may be almost negligible to the $NO_x$ removal compared with the day OH + $NO_2$ pathway according to previous works reported in urban regions (Wang et al., 2017b; Wang et al., 2020a). The diurnal variation of the $NO_3$ loss fraction of both periods was shown in Fig. 7c and 7d, revealing that $NO_3$ loss via $N_2O_5$ uptake and VOCs was slightly higher in the early evening and relatively stable in the late evening. The pie charts in the center were the relative contribution between VOCs and $N_2O_5$ uptake, showing that VOCs were overwhelming compared with $N_2O_5$ uptake during the two periods, with an average of 68.4% and 91.7% during the first and second periods, respectively.

To better understand the nocturnal oxidation of VOCs, we compared the nighttime oxidation of VOCs by $NO_3$ with $O_3$. Since OH was not measured and OH is often regarded as a vital daytime oxidant (Finlayson-Pitts, 2000; Lu et al., 2010), we did not consider OH oxidation in the nighttime. Figure S4 showed the diurnal pattern of VOC loss rate by $NO_3$ and $O_3$, $NO_3$ predominantly achieves its peak oxidation rates (0.07 ppbv $h^{-1}$) during the initial half of the night, accounting for 63.1% of the total VOC oxidation on nocturnal average. Meanwhile, $O_3$ also makes a contribution to VOC oxidation, mainly owing to its relatively high nighttime concentration levels (42.9 ± 18.4 ppbv).

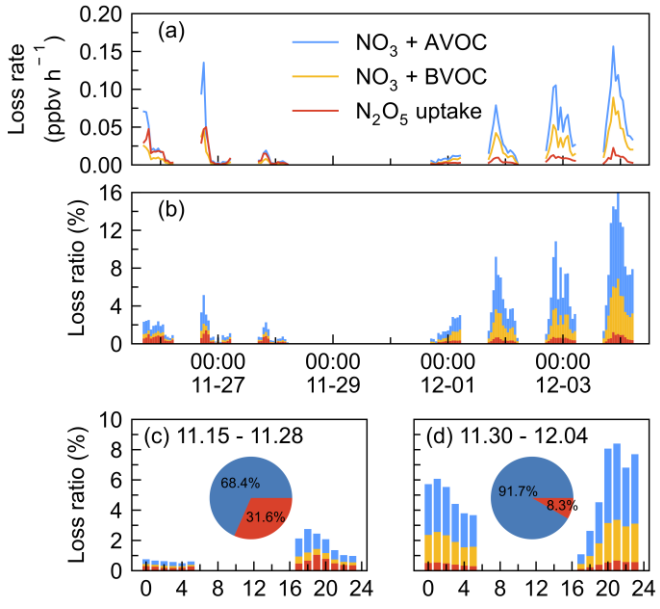


**Figure 7.** Time series of (a) the loss rate of $NO_3$ reactions with AVOC, BVOC, and $N_2O_5$

uptake, and (b) fractional contribution to the $NO_3$ loss during the nighttime by taking $P(NO_3)$ as the total $NO_3$ loss in the IAM period. The mean diurnal profiles of $NO_3$ loss ratio in two periods (c) November 25$^{th}$ - 28$^{th}$, and (d) November 30$^{th}$ - December 4$^{th}$. Pie charts in the center showed the relative contribution of VOCs (blue) and $N_2O_5$ uptake (red) in $NO_3$ loss.

Due to the difficulty in experimental quantifying $\gamma(N_2O_5)$, the estimation of $N_2O_5$ uptake in $NO_3$ loss may include some uncertainty. Considering the uncertainty both in parameterized $\gamma(N_2O_5)$ and the $NO_3$ reactivity calculation, three sensitivity tests were conducted to assess the uncertainty in period II because of the relatively high loss ratio in the above analysis (Fig. 8), and the three cases were used to represent the upper limit of their contribution to $NO_3$ loss. Case 1 represents the overrated contribution of $N_2O_5$ uptake by taking $\gamma(N_2O_5) = 0.08$, which was the high value reported in high $N_2O_5$ and $ClNO_2$ plume of Shenzhen (Niu et al., 2022) and approximately seven times the parameterized value at this site. In this case, the fraction of $NO_3$+VOCs and $N_2O_5$ uptake was significantly elevated to account for approximately 30% of $NO_3$ loss. Case 2 shows the total $NO_3$ reactivity reached an average of $5.0 \times 10^{-3}$ $s^{-1}$ by taking β-pinene as the total monoterpene because of the higher reaction rate constant. The weak change in the loss ratio indicates the reactions of $NO_3$ with VOC may not be sensitive to the weights of monoterpenes, since the contribution of monoterpenes to the $NO_3$ reactivity is not dominant. Case 3 is the synthesis of Case 1 and Case 2 by considering higher $N_2O_5$ uptake coefficient and higher $k(NO_3)$ to represent the upper limit of $N_2O_5$ uptake and $NO_3$ reaction with VOCs to $NO_3$ loss, whose result is slightly higher than the contribution of Case 1. Nevertheless, the quantified upper contribution was still less than half. Thus, we conclude that most of the $NO_3$ loss was not well accounted for even considering the uncertainties.

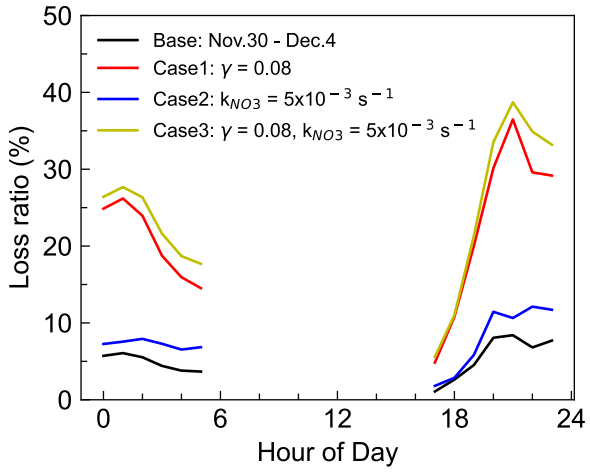


**Figure 8.** Three sensitivity tests for the contribution of VOCs and $N_2O_5$ uptake to the $NO_3$

loss during the nighttime of period II (November 30$^{th}$ - December 4$^{th}$). Case 1 takes $\gamma(N_2O_5)$ = 0.08, which is the high value reported in the previous study. Case 2 takes β-pinene as the total monoterpene with a higher reaction rate constant, and Case 3 is the synthesis of the above two cases to represent the upper limit of the contribution.

The $NO_3$ reaction with NO was often considered to be one of the dominant loss processes during the daytime since at nighttime NO decreased to low levels, thus not considered in the above analysis. However, by taking NO into consideration although at low concentration levels below the detection limit of the instrument (0.4 ppbv), the contribution of NO to the nighttime $NO_3$ loss exceeded 100% frequently as shown in Fig. S5. Due to the rapid reaction between NO and $NO_3$, several pptv concentrations of NO could effectively account for most $NO_3$ loss in a relatively clean coastal environment (Crowley et al., 2011). Nevertheless, limited by NO precise measurement, we considered the following assessments to understand the total $NO_3$ loss processes (Fig. 9). By assuming NO at a constant value of 40-400 pptv, more than 80% of the total $NO_3$ loss can be well explained. Although some loss remained unidentified, these results underline that NO, often considered to be important during daytime, was the predominant $NO_3$ loss way during nighttime at this study site. This also suggests accurate measurement of low NO concentrations is crucial for identifying removal pathways of nocturnal $NO_3$ oxidants and has significant implications for nighttime atmospheric chemistry. We can infer that the nocturnal chemical $NO_3$ reactions would be largely enhanced once without NO emission in the open ocean after the air mass passes through this site, indicating the strong influences of the urban outflow to the downwind marine areas with respect to nighttime chemistry.

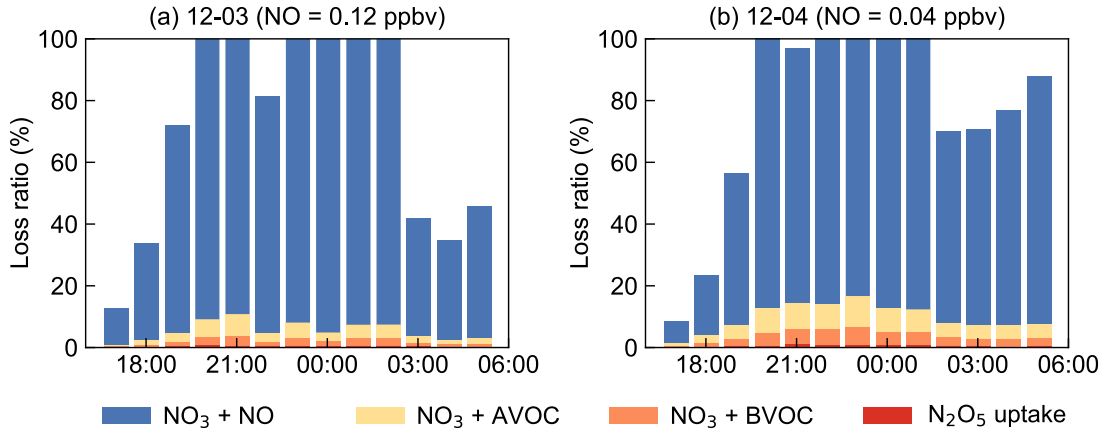


**Figure 9.** Examples for the assessment of $NO_3$ loss process by assuming NO as constant values to approximately explain about 80% of the budget.

For the absence of measured $N_2O_5$ during the CAM period, we compared the k($NO_3$) and the reactivity of $N_2O_5$ uptake ($k_{het}K_{eq}NO_2$) to indirectly reflect $NO_3$ removal process. Overall, the $NO_3$ reactivity values from VOCs and $N_2O_5$ uptake during nighttime were relatively comparable, for 56.5% and 43.5%, respectively. This indicates that VOCs still had a slightly larger contribution than $N_2O_5$ uptake during the CAM period, which is consistent with the findings in southern China (Brown et al., 2016) and on the east coast of the USA (Aldener et al., 2006).

## 4. Summary and Conclusion

This study presents the first observation of nocturnal nitrogen oxide species, $N_2O_5$, at a typical marine site (Da Wan Shan Island, Zhuhai) in the north of the South China Sea during the winter of 2021. Although Da Wan Shan Island was almost free of local anthropogenic emissions, the air pollutants from the megacities of the Pearl River Delta were transported to this area by northerly or northeasterly winds during the measurement period. The maximum ratio of $N_2O_5$ was 657.27 pptv (1 min average) and the nocturnal average was 119.5 ± 128.6 pptv. The $NO_3$ production rate was comparable to that in urban areas such as north China and the Yangtze River Delta, with an average value of 1.5 ± 0.9 ppbv $h^{-1}$ and a maximum of up to 5.84 ppbv $h^{-1}$, indicating an active nighttime chemical process in that area.

Further analysis of $N_2O_5$ and $NO_3$ steady state lifetimes indicates that $NO_3$ had a very short average life of 0.5 ± 0.6 minutes, which was to some extent comparable to that in urban areas in summer. The combination of the high $NO_3$ production rate and short lifetime suggests a rapid $NO_3$ loss at night. While $N_2O_5$ uptake is inefficient in relatively clean air masses. The nighttime k($NO_3$) corresponded to a $NO_3$ lifetime of 4.5 minutes, indicating that VOCs also contribute little to $NO_3$ loss. Both VOC and $N_2O_5$ uptake can only explain less than 20% of the total loss. The fast $NO_3$ loss rate also indicated the air mass that was influenced by local surface-level emissions. We infer that the local weak NO emission may significantly change the near-surface chemical pattern of $NO_3$ chemistry, which may result in a huge difference between the observed results on the island and those on the sea surface. We suggested that future field measurements should be made on sea surfaces away from islands, such as ship-based cruise observation, to get a comprehensive understanding of the nocturnal $NO_3$ chemistry in the background marine regions.

**Code/Data availability.** The datasets used in this study are available at: https://doi.org/10.5281/zenodo.8089100 (Wang et al., 2023).

**Author contributions.** H.C.W. and Y. J.T. designed the study. J.W. and H.C.W. analyzed the data with input from H.J.H., Z.L.Z., G.Z.F., C.Z.S., Z.H.L., J.Z., S.J.F.. H.C.W., L.M. Y. J.T., Z.H.L., and J.Z. organized this field campaign and provided the field measurement dataset. J.W., H.C.W., and Y.J.T. wrote the paper. All authors commented on and edited the manuscript.


## Acknowledgments

This work was supported by the National Natural Science Foundation of China (Nos. 42175111), the Guangdong Major Project of Basic and Applied Basic Research (No. 2020B0301030004), Guangdong Basic and Applied Basic Research Foundation (2022A1515010852), and the Fundamental Research Funds for the Central Universities, Sun Yat-sen University (23lgbj002, 23hytd002). L.M. acknowledges the Zhuhai Science and Technology Plan Project (ZH22036201210115PWC).


**Competing interests**. The authors declare that they have no conflicts of interest.

## Appendix A Supplementary data

Supplementary data associated with this article can be found in the online version at xxxxxx.

## Reference


Aldener, M., Brown, S. S., Stark, H., Williams, E. J., Lerner, B. M., Kuster, W. C., Goldan, P. D., Quinn, P. K., Bates, T. S., Fehsenfeld, F. C., and Ravishankara, A. R.: Reactivity and loss mechanisms of $NO_3$ and $N_2O_5$ in a polluted marine environment: Results from in situ measurements during New England Air Quality Study 2002, Journal of Geophysical Research-Atmospheres, 111, Artn D23s73, Doi 10.1029/2006jd007252, 2006.

Allan, B. J., Carslaw, N., Coe, H., Burgess, R. A., and Plane, J. M. C.: Observations of the nitrate radical in the marine boundary layer, Journal of Atmospheric Chemistry, 33, 129-154, Doi 10.1023/A:1005917203307, 1999.

Atkinson, R., Baulch, D. L., Cox, R. A., Crowley, J. N., Hampson, R. F., Hynes, R. G., Jenkin, M. E., Rossi, M. J., and Troe, J.: Evaluated kinetic and photochemical data for atmospheric chemistry: Volume I - gas phase reactions of $O_x$, $HO_x$, $NO_x$ and $SO_x$ species, Atmospheric Chemistry and Physics, 4, 1461-1738, DOI 10.5194/acp-4-1461-2004, 2004.

Ayres, B. R., Allen, H. M., Draper, D. C., Brown, S. S., Wild, R. J., Jimenez, J. L., Day, D. A., Campuzano-Jost, P., Hu, W., de Gouw, J., Koss, A., Cohen, R. C., Duffey, K. C., Romer, P., Baumann, K., Edgerton, E., Takahama, S., Thornton, J. A., Lee, B. H., Lopez-Hilfiker, F. D., Mohr, C., Wennberg, P. O., Nguyen, T. B., Teng, A., Goldstein, A. H., Olson, K., and Fry, J. L.: Organic nitrate aerosol formation via $NO_3$ + biogenic volatile organic compounds in the southeastern United States, Atmospheric Chemistry

and Physics, 15, 13377-13392, 10.5194/acp-15-13377-2015, 2015.
Behnke, W., and, V., Scheer, and, C., and Zetzsch: 16 O 04 Formation of $ClNO_2$ and $HNO_3$ in the presence of $N_2O_5$ and wet pure NaCl- and wet mixed $NaCl/Na_2SO_4$- aerosol, J Aerosol Sci, 24, S115-S116, 1993.
Bertram, T. H. and Thornton, J. A.: Toward a general parameterization of $N_2O_5$ reactivity on aqueous particles: the competing effects of particle liquid water, nitrate and chloride, Atmospheric Chemistry and Physics, 9, 8351-8363, 2009.
Brown, S. S. and Stutz, J.: Nighttime radical observations and chemistry, Chem Soc Rev, 41, 6405-6447, Doi 10.1039/C2cs35181a, 2012.
Brown, S. S., Stark, H., and Ravishankara, A. R.: Applicability of the steady state approximation to the interpretation of atmospheric observations of $NO_3$ and $N_2O_5$, Journal of Geophysical Research-Atmospheres, 108, Artn 4539, Doi 10.1029/2003jd003407, 2003.
Brown, S. S., Dube, W. P., Tham, Y. J., Zha, Q. Z., Xue, L. K., Poon, S., Wang, Z., Blake, D. R., Tsui, W., Parrish, D. D., and Wang, T.: Nighttime chemistry at a high altitude site above Hong Kong, Journal of Geophysical Research-Atmospheres, 121, 2457-2475, 10.1002/2015jd024566, 2016.
Brown, S. S., Ryerson, T. B., Wollny, A. G., Brock, C. A., Peltier, R., Sullivan, A. P., Weber, R. J., Dube, W. P., Trainer, M., Meagher, J. F., Fehsenfeld, F. C., and Ravishankara, A. R.: Variability in nocturnal nitrogen oxide processing and its role in regional air quality, Science, 311, 67-70, DOI 10.1126/science.1120120, 2006.
Brown, S. S., Dube, W. P., Peischl, J., Ryerson, T. B., Atlas, E., Warneke, C., de Gouw, J. A., Hekkert, S. T., Brock, C. A., Flocke, F., Trainer, M., Parrish, D. D., Feshenfeld, F. C., and Ravishankara, A. R.: Budgets for nocturnal VOC oxidation by nitrate radicals aloft during the 2006 Texas Air Quality Study, Journal of Geophysical Research-Atmospheres, 116, Artn D24305, 10.1029/2011jd016544, 2011.
Brown, S. S., Dube, W. P., Fuchs, H., Ryerson, T. B., Wollny, A. G., Brock, C. A., Bahreini, R., Middlebrook, A. M., Neuman, J. A., Atlas, E., Roberts, J. M., Osthoff, H. D., Trainer, M., Fehsenfeld, F. C., and Ravishankara, A. R.: Reactive uptake coefficients for N2O5 determined from aircraft measurements during the Second Texas Air Quality Study: Comparison to current model parameterizations, Journal of Geophysical Research-Atmospheres, 114, Artn D00f10, 10.1029/2008jd011679, 2009.
Brown, S. S., Dube, W. P., Osthoff, H. D., Stutz, J., Ryerson, T. B., Wollny, A. G., Brock, C. A., Warneke, C., De Gouw, J. A., Atlas, E., Neuman, J. A., Holloway, J. S., Lerner, B. M., Williams, E. J., Kuster, W. C., Goldan, P. D., Angevine, W. M., Trainer, M., Fehsenfeld, F. C., and Ravishankara, A. R.: Vertical profiles in $NO_3$ and $N_2O_5$ measured from an aircraft: Results from the NOAA P-3 and surface platforms during the New England Air Quality Study 2004, Journal of Geophysical Research-Atmospheres, 112, Artn D22304, 10.1029/2007jd008883, 2007.

Brown, S. S., Dibb, J. E., Stark, H., Aldener, M., Vozella, M., Whitlow, S., Williams, E. J., Lerner, B. M., Jakoubek, R., Middlebrook, A. M., DeGouw, J. A., Warneke, C., Goldan, P. D., Kuster, W. C., Angevine, W. M., Sueper, D. T., Quinn, P. K., Bates, T. S., Meagher, J. F., Fehsenfeld, F. C., and Ravishankara, A. R.: Nighttime removal of NOx in the summer marine boundary layer, Geophysical Research Letters, 31, Artn L07108, Doi 10.1029/2004gl019412, 2004.

Chen, X., Wang, H., and Lu, K.: Interpretation of $NO_3$–$N_2O_5$ observation via steady state in high-aerosol air mass: the impact of equilibrium coefficient in ambient conditions, Atmospheric Chemistry and Physics, 22, 3525-3533, 10.5194/acp-22-3525-2022, 2022.

Chuang, M.-T., Chang, S.-C., Lin, N.-H., Wang, J.-L., Sheu, G.-R., Chang, Y.-J., and Lee, C.-T.: Aerosol chemical properties and related pollutants measured in Dongsha Island in the northern South China Sea during 7-SEAS/Dongsha Experiment, Atmospheric Environment, 78, 82-92, 10.1016/j.atmosenv.2012.05.014, 2013.

Crowley, J. N., Thieser, J., Tang, M. J., Schuster, G., Bozem, H., Beygi, Z. H., Fischer, H., Diesch, J. M., Drewnick, F., Borrmann, S., Song, W., Yassaa, N., Williams, J., Pohler, D., Platt, U., and Lelieveld, J.: Variable lifetimes and loss mechanisms for $NO_3$ and $N_2O_5$ during the DOMINO campaign: contrasts between marine, urban and continental air, Atmospheric Chemistry and Physics, 11, 10853-10870, 10.5194/acp-11-10853-2011, 2011.

Delhomme, O., Morville, S., and Millet, M.: Seasonal and diurnal variations of atmospheric concentrations of phenols and nitrophenols measured in the Strasbourg area, France, Atmospheric Pollution Research, 1, 16-22, 10.5094/apr.2010.003, 2010.

Dewald, P., Nussbaumer, C. M., Schuladen, J., Ringsdorf, A., Edtbauer, A., Fischer, H., Williams, J., Lelieveld, J., and Crowley, J. N.: Fate of the nitrate radical at the summit of a semi-rural mountain site in Germany assessed with direct reactivity measurements, Atmospheric Chemistry and Physics, 22, 7051-7069, 10.5194/acp-22-7051-2022, 2022.

Edwards, P. M., Aikin, K. C., Dube, W. P., Fry, J. L., Gilman, J. B., de Gouw, J. A., Graus, M. G., Hanisco, T. F., Holloway, J., Huber, G., Kaiser, J., Keutsch, F. N., Lerner, B. M., Neuman, J. A., Parrish, D. D., Peischl, J., Pollack, I. B., Ravishankara, A. R., Roberts, J. M., Ryerson, T. B., Trainer, M., Veres, P. R., Wolfe, G. M., Warneke, C., and Brown, S. S.: Transition from high- to low-$NO_x$ control of night-time oxidation in the southeastern US, Nat Geosci, 10, 490-+, 10.1038/Ngeo2976, 2017.

Evans, M. J. and Jacob, D. J.: Impact of new laboratory studies of $N_2O_5$ hydrolysis on global model budgets of tropospheric nitrogen oxides, ozone, and OH, Geophysical Research Letters, 32, Artn L09813, Doi 10.1029/2005gl022469, 2005.

Finlayson-Pitts, B. J., James N.: Chemistry of the upper and lower atmosphere: theory, experiments and applications, Academic Press, Calif2000.

Fuentes., J. D., Lerdau., M., and Atkinson., R.: Biogenic_hydrocarbons_in_the_atmospheric_Boundary_A review, B Am Meteorol Soc, 2000.

Geyer, A., Alicke, B., Konrad, S., Schmitz, T., Stutz, J., and Platt, U.: Chemistry and oxidation capacity of the nitrate radical in the continental boundary layer near Berlin, Journal of Geophysical Research-Atmospheres, 106, 8013-8025, Doi 10.1029/2000jd900681, 2001.

Gu, S., Guenther, A., and Faiola, C.: Effects of Anthropogenic and Biogenic Volatile Organic Compounds on Los Angeles Air Quality, Environ Sci Technol, 55, 12191-12201, 10.1021/acs.est.1c01481, 2021.

Hallquist, M., Stewart, D. J., Stephenson, S. K., and Cox, R. A.: Hydrolysis of $N_2O_5$ on sub-micron sulfate aerosols, Phys Chem Chem Phys, 5, 3453-3463, Doi 10.1039/B301827j, 2003.

Ian Barnes, Jens Hjorth, and Mihalopoulos, N.: Dimethyl Sulfide and Dimethyl Sulfoxide and Their Oxidation in the Atmosphere, Chem Rev, 2006.

Kane, S. M., Caloz, F., and Leu, M. T.: Heterogeneous uptake of gaseous $N_2O_5$ by $(NH_4)(2)SO_4$, $NH_4HSO_4$, and $H_2SO_4$ aerosols, J Phys Chem A, 105, 6465-6470, Doi 10.1021/Jp010490x, 2001.

Kiendler-Scharr, A., Mensah, A. A., Friese, E., Topping, D., Nemitz, E., Prevot, A. S. H., Aijala, M., Allan, J., Canonaco, F., Canagaratna, M., Carbone, S., Crippa, M., Dall Osto, M., Day, D. A., De Carlo, P., Di Marco, C. F., Elbern, H., Eriksson, A., Freney, E., Hao, L., Herrmann, H., Hildebrandt, L., Hillamo, R., Jimenez, J. L., Laaksonen, A., McFiggans, G., Mohr, C., O'Dowd, C., Otjes, R., Ovadnevaite, J., Pandis, S. N., Poulain, L., Schlag, P., Sellegri, K., Swietlicki, E., Tiitta, P., Vermeulen, A., Wahner, A., Worsnop, D., and Wu, H. C.: Ubiquity of organic nitrates from nighttime chemistry in the European submicron aerosol, Geophysical Research Letters, 43, 7735-7744, 10.1002/2016gl069239, 2016.

Li, Z., Xie, P., Hu, R., Wang, D., Jin, H., Chen, H., Lin, C., and Liu, W.: Observations of $N_2O_5$ and $NO_3$ at a suburban environment in Yangtze river delta in China: Estimating heterogeneous $N_2O_5$ uptake coefficients, J Environ Sci (China), 95, 248-255, 10.1016/j.jes.2020.04.041, 2020.

Liebmann, J., Karu, E., Sobanski, N., Schuladen, J., Ehn, M., Schallhart, S., Quelever, L., Hellen, H., Hakola, H., Hoffmann, T., Williams, J., Fischer, H., Lelieveld, J., and Crowley, J. N.: Direct measurement of $NO_3$ radical reactivity in a boreal forest, Atmospheric Chemistry and Physics, 18, 3799-3815, 10.5194/acp-18-3799-2018, 2018a.

Liebmann, J. M., Muller, J. B. A., Kubistin, D., Claude, A., Holla, R., Plass-Dulmer, C., Lelieveld, J., and Crowley, J. N.: Direct measurements of $NO_3$ reactivity in and above the boundary layer of a mountaintop site: identification of reactive trace gases and

774 comparison with OH reactivity, Atmospheric Chemistry and Physics, 18, 12045-
775 12059, 10.5194/acp-18-12045-2018, 2018b.
776 Lin, C., Hu, R., Xie, P., Lou, S., Zhang, G., Tong, J., Liu, J., and Liu, W.: Nocturnal
777 atmospheric chemistry of $NO_3$ and $N_2O_5$ over Changzhou in the Yangtze River Delta
778 in China, J Environ Sci (China), 114, 376-390, 10.1016/j.jes.2021.09.016, 2022.
779 Liu, X., Lyu, X., Wang, Y., Jiang, F., and Guo, H.: Intercomparison of $O_3$ formation and
780 radical chemistry in the past decade at a suburban site in Hong Kong, Atmospheric
781 Chemistry and Physics, 19, 5127-5145, 10.5194/acp-19-5127-2019, 2019.
782 Liu, X. G., Gu, J. W., Li, Y. P., Cheng, Y. F., Qu, Y., Han, T. T., Wang, J. L., Tian, H. Z.,
783 Chen, J., and Zhang, Y. H.: Increase of aerosol scattering by hygroscopic growth:
784 Observation, modeling, and implications on visibility, Atmospheric Research, 132,
785 91-101, 10.1016/j.atmosres.2013.04.007, 2013.
786 Lu, K. D., Zhang, Y. H., Su, H., Brauers, T., Chou, C. C., Hofzumahaus, A., Liu, S. C., Kita,
787 K., Kondo, Y., Shao, M., Wahner, A., Wang, J. L., Wang, X. S., and Zhu, T.: Oxidant
788 ($O_3$ + $NO_2$) production processes and formation regimes in Beijing, Journal of
789 Geophysical Research-Atmospheres, 115, Artn D07303, 10.1029/2009jd012714,
790 2010.
791 Lu, X., Qin, M., Xie, P., Duan, J., Fang, W., and Liu, W.: Observation of ambient $NO_3$
792 radicals by LP-DOAS at a rural site in North China Plain, Sci Total Environ, 804,
793 149680, 10.1016/j.scitotenv.2021.149680, 2022.
794 Lüttke, J., Scheer, V., Levsen, K., Wünsch, G., Cape, J. N., Hargreaves, K. J., Storeton-
795 West, R. L., Acker, K., Wieprecht, W., and Jones, B.: Occurrence and formation of
796 nitrated phenols in and out of cloud, Atmospheric Environment, 31, 2637-2648, 1997.
797 McMurry, P. H., Woo, K. S., Weber, R., Chen, D. R., and Pui, D. Y. H.: Size distributions
798 of 3-10 nm atmospheric particles: implications for nucleation mechanisms,
799 Philosophical Transactions of the Royal Society a-Mathematical Physical and
800 Engineering Sciences, 358, 2625-2642, 10.1098/rsta.2000.0673, 2000.
801 Mogensen, D., Gierens, R., Crowley, J. N., Keronen, P., Smolander, S., Sogachev, A.,
802 Nolscher, A. C., Zhou, L., Kulmala, M., Tang, M. J., Williams, J., and Boy, M.:
803 Simulations of atmospheric OH, $O_3$ and $NO_3$ reactivities within and above the boreal
804 forest, Atmospheric Chemistry and Physics, 15, 3909-3932, 10.5194/acp-15-3909-
805 2015, 2015.
806 Morgan, W. T., Ouyang, B., Allan, J. D., Aruffo, E., Di Carlo, P., Kennedy, O. J., Lowe, D.,
807 Flynn, M. J., Rosenberg, P. D., Williams, P. I., Jones, R., McFiggans, G. B., and Coe,
808 H.: Influence of aerosol chemical composition on $N_2O_5$ uptake: airborne regional
809 measurements in northwestern Europe, Atmospheric Chemistry and Physics, 15, 973-
810 990, DOI 10.5194/acp-15-973-2015, 2015.
811 Ng, N. L., Brown, S. S., Archibald, A. T., Atlas, E., Cohen, R. C., Crowley, J. N., Day, D.
812 A., Donahue, N. M., Fry, J. L., Fuchs, H., Griffin, R. J., Guzman, M. I., Herrmann, H.,

Hodzic, A., Iinuma, Y., Jimenez, J. L., Kiendler-Scharr, A., Lee, B. H., Luecken, D. J., Mao, J. Q., McLaren, R., Mutzel, A., Osthoff, H. D., Ouyang, B., Picquet-Varrault, B., Platt, U., Pye, H. O. T., Rudich, Y., Schwantes, R. H., Shiraiwa, M., Stutz, J., Thornton, J. A., Tilgner, A., Williams, B. J., and Zaveri, R. A.: Nitrate radicals and biogenic volatile organic compounds: oxidation, mechanisms, and organic aerosol, Atmospheric Chemistry and Physics, 17, 2103-2162, 10.5194/acp-17-2103-2017, 2017.

Niu, Y. B., Zhu, B., He, L. Y., Wang, Z., Lin, X. Y., Tang, M. X., and Huang, X. F.: Fast Nocturnal Heterogeneous Chemistry in a Coastal Background Atmosphere and Its Implications for Daytime Photochemistry, Journal of Geophysical Research: Atmospheres, 127, 10.1029/2022jd036716, 2022.

Osthoff, H. D., Pilling, M. J., Ravishankara, A. R., and Brown, S. S.: Temperature dependence of the $NO_3$ absorption cross-section above 298 K and determination of the equilibrium constant for $NO_3 + NO_2 \rightarrow N_2O_5$ at atmospherically relevant conditions, Phys Chem Chem Phys, 9, 5785-5793, 10.1039/b709193a, 2007.

Osthoff, H. D., Roberts, J. M., Ravishankara, A. R., Williams, E. J., Lerner, B. M., Sommariva, R., Bates, T. S., Coffman, D., Quinn, P. K., Dibb, J. E., Stark, H., Burkholder, J. B., Talukdar, R. K., Meagher, J., Fehsenfeld, F. C., and Brown, S. S.: High levels of nitryl chloride in the polluted subtropical marine boundary layer, Nat Geosci, 1, 324-328, Doi 10.1038/Ngeo177, 2008.

Riedel, T. P., Bertram, T. H., Crisp, T. A., Williams, E. J., Lerner, B. M., Vlasenko, A., Li, S. M., Gilman, J., de Gouw, J., Bon, D. M., Wagner, N. L., Brown, S. S., and Thornton, J. A.: Nitryl Chloride and Molecular Chlorine in the Coastal Marine Boundary Layer, Environmental Science & Technology, 46, 10463-10470, 10.1021/es204632r, 2012.

Riedel, T. P., Wolfe, G. M., Danas, K. T., Gilman, J. B., Kuster, W. C., Bon, D. M., Vlasenko, A., Li, S. M., Williams, E. J., Lerner, B. M., Veres, P. R., Roberts, J. M., Holloway, J. S., Lefer, B., Brown, S. S., and Thornton, J. A.: An MCM modeling study of nitryl chloride ($ClNO_2$) impacts on oxidation, ozone production and nitrogen oxide partitioning in polluted continental outflow, Atmospheric Chemistry and Physics, 14, 3789-3800, 10.5194/acp-14-3789-2014, 2014.

Rosati, B., Isokääntä, S., Christiansen, S., Jensen, M. M., Moosakutty, S. P., Wollesen de Jonge, R., Massling, A., Glasius, M., Elm, J., Virtanen, A., and Bilde, M.: Hygroscopicity and CCN potential of DMS-derived aerosol particles, Atmospheric Chemistry and Physics, 22, 13449-13466, 10.5194/acp-22-13449-2022, 2022.

Tang, M. J., Schuster, G., and Crowley, J. N.: Heterogeneous reaction of N2O5 with illite and Arizona test dust particles, Atmospheric Chemistry and Physics, 14, 245-254, DOI 10.5194/acp-14-245-2014, 2014.

Tham, Y. J., Wang, Z., Li, Q., Wang, W., Wang, X., Lu, K., Ma, N., Yan, C., Kecorius, S., Wiedensohler, A., Zhang, Y., and Wang, T.: Heterogeneous $N_2O_5$ uptake coefficient

and production yield of $ClNO_2$ in polluted northern China: roles of aerosol water content and chemical composition, Atmos. Chem. Phys., 18, 13155-13171, 10.5194/acp-18-13155-2018, 2018.

Tham, Y. J., Wang, Z., Li, Q. Y., Yun, H., Wang, W. H., Wang, X. F., Xue, L. K., Lu, K. D., Ma, N., Bohn, B., Li, X., Kecorius, S., Gross, J., Shao, M., Wiedensohler, A., Zhang, Y. H., and Wang, T.: Significant concentrations of nitryl chloride sustained in the morning: investigations of the causes and impacts on ozone production in a polluted region of northern China, Atmospheric Chemistry and Physics, 16, 14959-14977, 10.5194/acp-16-14959-2016, 2016.

Thornton, J. A., Kercher, J. P., Rie De L, T. P., Wagner, N. L., Cozic, J., Holloway, J. S., Dubé, W., Wolfe, G. M., Quinn, P. K., and Middlebrook, A. M.: A large atomic chlorine source inferred from mid-continental reactive nitrogen chemistry, Nature, 464, 271-274, 2010.

Vrekoussis, M., Mihalopoulos, N., Gerasopoulos, E., Kanakidou, M., Crutzen, P. J., and Lelieveld, J.: Two-years of $NO_3$ radical observations in the boundary layer over the Eastern Mediterranean, Atmospheric Chemistry and Physics, 7, 315-327, 2007.

Vrekoussis, M., Kanakidou, M., Mihalopoulos, N., Crutzen, P. J., Lelieveld, J., Perner, D., Berresheim, H., and Baboukas, E.: Role of the $NO_3$ radicals in oxidation processes in the eastern Mediterranean troposphere during the MINOS campaign, Atmospheric Chemistry and Physics, 4, 169-182, 2004.

Wagner, N. L., Riedel, T. P., Young, C. J., Bahreini, R., Brock, C. A., Dube, W. P., Kim, S., Middlebrook, A. M., Ozturk, F., Roberts, J. M., Russo, R., Sive, B., Swarthout, R., Thornton, J. A., VandenBoer, T. C., Zhou, Y., and Brown, S. S.: $N_2O_5$ uptake coefficients and nocturnal $NO_2$ removal rates determined from ambient wintertime measurements, Journal of Geophysical Research-Atmospheres, 118, 9331-9350, Doi 10.1002/Jgrd.50653, 2013.

Wang, H., Chen, J., and Lu, K.: Development of a portable cavity-enhanced absorption spectrometer for the measurement of ambient $NO_3$ and $N_2O_5$: experimental setup, lab characterizations, and field applications in a polluted urban environment, Atmos Meas Tech, 10, 1465-1479, 10.5194/amt-10-1465-2017, 2017a.

Wang, H., Chen, T., and Lu, K.: Measurement of $NO_3$ and $N_2O_5$ in the Troposphere, Progress in Chemistry, 27, 963-976, 10.7536/pc141230, 2015.

Wang, H., Lu, K., Chen, S., Li, X., Zeng, L., Hu, M., and Zhang, Y.: Characterizing nitrate radical budget trends in Beijing during 2013–2019, Science of The Total Environment, 795, 10.1016/j.scitotenv.2021.148869, 2021.

Wang, H., Wang, H., Lu, X., Lu, K., Zhang, L., Tham, Y. J., Shi, Z., Aikin, K., Fan, S., Brown, S. S., and Zhang, Y.: Increased night-time oxidation over China despite widespread decrease across the globe, Nat Geosci, 10.1038/s41561-022-01122-x, 2023.

Wang, H., Lyu, X., Guo, H., Wang, Y., Zou, S., Ling, Z., Wang, X., Jiang, F., Zeren, Y., Pan, W., Huang, X., and Shen, J.: WS-Ozone pollution around a coastal region of South China Sea: interaction between marine and continental air, Atmospheric Chemistry and Physics, 18, 4277-4295, 10.5194/acp-18-4277-2018, 2018a.

Wang, H., Chen, X., Lu, K., Hu, R., Li, Z., Wang, H., Ma, X., Yang, X., Chen, S., Dong, H., Liu, Y., Fang, X., Zeng, L., Hu, M., and Zhang, Y.: $NO_3$ and $N_2O_5$ chemistry at a suburban site during the EXPLORE-YRD campaign in 2018, Atmospheric Environment, 224, 10.1016/j.atmosenv.2019.117180, 2020a.

Wang, H., Chen, X., Lu, K., Tan, Z., Ma, X., Wu, Z., Li, X., Liu, Y., Shang, D., Wu, Y., Zeng, L., Hu, M., Schmitt, S., Kiendler-Scharr, A., Wahner, A., and Zhang, Y.: Wintertime $N_2O_5$ uptake coefficients over the North China Plain, Science Bulletin, 65, 765-774, 10.1016/j.scib.2020.02.006, 2020b.

Wang, H., Lu, K., Guo, S., Wu, Z., Shang, D., Tan, Z., Wang, Y., Le Breton, M., Lou, S., Tang, M., Wu, Y., Zhu, W., Zheng, J., Zeng, L., Hallquist, M., Hu, M., and Zhang, Y.: Efficient $N_2O_5$ uptake and $NO_3$ oxidation in the outflow of urban Beijing, Atmospheric Chemistry and Physics, 18, 9705-9721, 10.5194/acp-18-9705-2018, 2018b.

Wang, H., Lu, K., Chen, X., Zhu, Q., Chen, Q., Guo, S., Jiang, M., Li, X., Shang, D., Tan, Z., Wu, Y., Wu, Z., Zou, Q., Zheng, Y., Zeng, L., Zhu, T., Hu, M., and Zhang, Y.: High $N_2O_5$ Concentrations Observed in Urban Beijing: Implications of a Large Nitrate Formation Pathway, Environmental Science & Technology Letters, 4, 416-420, 10.1021/acs.estlett.7b00341, 2017b.

Wang, H., Yuan, B., Zheng, E., Zhang, X., Wang, J., Lu, K., Ye, C., Yang, L., Huang, S., Hu, W., Yang, S., Peng, Y., Qi, J., Wang, S., He, X., Chen, Y., Li, T., Wang, W., Huangfu, Y., Li, X., Cai, M., Wang, X., and Shao, M.: Formation and impacts of nitryl chloride in Pearl River Delta, Atmospheric Chemistry and Physics, 22, 14837-14858, 10.5194/acp-22-14837-2022, 2022.

Wang, S. S., Shi, C. Z., Zhou, B., Zhao, H., Wang, Z. R., Yang, S. N., and Chen, L. M.: Observation of $NO_3$ radicals over Shanghai, China, Atmospheric Environment, 70, 401-409, DOI 10.1016/j.atmosenv.2013.01.022, 2013.

Wang, X. F., Wang, H., Xue, L. K., Wang, T., Wang, L. W., Gu, R. R., Wang, W. H., Tham, Y. J., Wang, Z., Yang, L. X., Chen, J. M., and Wang, W. X.: Observations of $N_2O_5$ and $ClNO_2$ at a polluted urban surface site in North China: High $N_2O_5$ uptake coefficients and low $ClNO_2$ product yields, Atmospheric Environment, 156, 125-134, 10.1016/j.atmosenv.2017.02.035, 2017c.

Wang, Z., Wang, W. H., Tham, Y. J., Li, Q. Y., Wang, H., Wen, L., Wang, X. F., and Wang, T.: Fast heterogeneous $N_2O_5$ uptake and $ClNO_2$ production in power plant and industrial plumes observed in the nocturnal residual layer over the North China Plain, Atmospheric Chemistry and Physics, 17, 12361-12378, 10.5194/acp-17-12361-2017,

2017d.
Wang, J., Wang, H., Tham, Y. J., Ming, L., Zheng, Z., Fang, G., Sun, C., Ling, Z., Zhao, J., and Fan, S.. (2023). Measurement report: Atmospheric nitrate radical chemistry in the South China Sea influenced by the urban outflow of the Pearl River Delta [Data set]. Zenodo. https://doi.org/10.5281/zenodo.8089100.
Wayne, R. P., Barnes, I., Biggs, P., Burrows, J. P., Canosamas, C. E., Hjorth, J., Lebras, G., Moortgat, G. K., Perner, D., Poulet, G., Restelli, G., and Sidebottom, H.: The Nitrate Radical - Physics, Chemistry, and the Atmosphere, Atmos Environ a-Gen, 25, 1-203, Doi 10.1016/0960-1686(91)90192-A, 1991.
Wood, E. C., Bertram, T. H., Wooldridge, P. J., and Cohen, R. C.: Measurements of $N_2O_5$, $NO_2$, and $O_3$ east of the San Francisco Bay, 2005.
Xu, L., Guo, H., Boyd, C. M., Klein, M., Bougiatioti, A., Cerully, K. M., Hite, J. R., Isaacman-VanWertz, G., Kreisberg, N. M., Knote, C., Olson, K., Koss, A., Goldstein, A. H., Hering, S. V., de Gouw, J., Baumann, K., Lee, S. H., Nenes, A., Weber, R. J., and Ng, N. L.: Effects of anthropogenic emissions on aerosol formation from isoprene and monoterpenes in the southeastern United States (vol 112, pg 37, 2015), P Natl Acad Sci USA, 112, E4506-E4507, 2015.
Yan, C., Tham, Y. J., Zha, Q. Z., Wang, X. F., Xue, L. K., Dai, J. N., Wang, Z., and Wang, T.: Fast heterogeneous loss of $N_2O_5$ leads to significant nighttime $NO_x$ removal and nitrate aerosol formation at a coastal background environment of southern China, Science of the Total Environment, 677, 637-647, 10.1016/j.scitotenv.2019.04.389, 2019.
Yan, Y., Wang, S., Zhu, J., Guo, Y., Tang, G., Liu, B., An, X., Wang, Y., and Zhou, B.: Vertically increased $NO_3$ radical in the nocturnal boundary layer, Sci Total Environ, 763, 142969, 10.1016/j.scitotenv.2020.142969, 2021.
Yang, S., Yuan, B., Peng, Y., Huang, S., Chen, W., Hu, W., Pei, C., Zhou, J., Parrish, D. D., Wang, W., He, X., Cheng, C., Li, X.-B., Yang, X., Song, Y., Wang, H., Qi, J., Wang, B., Wang, C., Wang, C., Wang, Z., Li, T., Zheng, E., Wang, S., Wu, C., Cai, M., Ye, C., Song, W., Cheng, P., Chen, D., Wang, X., Zhang, Z., Wang, X., Zheng, J., and Shao, M.: The formation and mitigation of nitrate pollution: comparison between urban and suburban environments, Atmospheric Chemistry and Physics, 22, 4539-4556, 10.5194/acp-22-4539-2022, 2022.
Yu, C., Wang, Z., Xia, M., Fu, X., Wang, W., Tham, Y. J., Chen, T., Zheng, P., Li, H., Shan, Y., Wang, X., Xue, L., Zhou, Y., Yue, D., Ou, Y., Gao, J., Lu, K., Brown, S. S., Zhang, Y., and Wang, T.: Heterogeneous $N_2O_5$ reactions on atmospheric aerosols at four Chinese sites: improving model representation of uptake parameters, Atmos. Chem. Phys., 20, 4367-4378, 10.5194/acp-20-4367-2020, 2020.
Yun, H., Wang, T., Wang, W. H., Tham, Y. J., Li, Q. Y., Wang, Z., and Poon, S. C. N.: Nighttime $NO_x$ loss and $ClNO_2$ formation in the residual layer of a polluted region:

Insights from field measurements and an iterative box model, Science of the Total Environment, 622, 727-734, 10.1016/j.scitotenv.2017.11.352, 2018a.

Yun, H., Wang, W. H., Wang, T., Xia, M., Yu, C., Wang, Z., Poon, S. C. N., Yue, D. L., and Zhou, Y.: Nitrate formation from heterogeneous uptake of dinitrogen pentoxide during a severe winter haze in southern China, Atmospheric Chemistry and Physics, 18, 17515-17527, 10.5194/acp-18-17515-2018, 2018b.

Zhou, W., Zhao, J., Ouyang, B., Mehra, A., Xu, W. Q., Wang, Y. Y., Bannan, T. J., Worrall, S. D., Priestley, M., Bacak, A., Chen, Q., Xie, C. H., Wang, Q. Q., Wang, J. F., Du, W., Zhang, Y. J., Ge, X. L., Ye, P. L., Lee, J. D., Fu, P. Q., Wang, Z. F., Worsnop, D., Jones, R., Percival, C. J., Coe, H., and Sun, Y. L.: Production of $N_2O_5$ and $ClNO_2$ in summer in urban Beijing, China, Atmospheric Chemistry and Physics, 18, 11581-11597, 10.5194/acp-18-11581-2018, 2018.

Zhu, J., Wang, S., Zhang, S., Xue, R., Gu, C., and Zhou, B.: Changes in $NO_3$ Radical and Its Nocturnal Chemistry in Shanghai From 2014 to 2021 Revealed by Long‐Term Observation and a Stacking Model: Impact of China's Clean Air Action Plan, Journal of Geophysical Research: Atmospheres, 127, 10.1029/2022jd037438, 2022.